

## Final Project Report Detailed Form

### I. Title of Proposed Project:

Smart Lighting for Internet of Things and Smart Homes

### II. Project Leader:

Full name: Pham Tien Dat

Institution: National Institute of Information and Communication Technology

Address: 4-2-1, Nukui-Kitamachi, Koganei, Tokyo 184-8795, Japan

Phone: +81-42-327-7300

E-mail: ptdat@nict.go.jp

### III. Project Members:

Name	Position/Degree	Department, Institution, Country	Email Address
Pham Tien Dat	Senior Researcher/PhD	National Institute of Information and Communication Technology (NICT), Japan	ptdat@nict.go.jp
Pham Quang Thai	Lecturer/PhD	Ho Chi Minh City University of Technology (HCMUT), Vietnam	pqthai@hcmut.edu.vn
Yusuf Nur Wijayanto	Researcher/PhD	Indonesian Institute of Sciences (LIPI), Indonesia	yusuf.nur.wijayanto@lipi.go.id
Dang The Ngoc	Department Head, Associate Professor/PhD	Posts and Telecommunications Institute of Technology (PTIT), Vietnam	ngocdt@ptit.edu.vn
Jiang Liu	Associate Professor/PhD	Faculty of Science and Engineering, Waseda University, Japan	liujiang@aoni.waseda.jp
Purwoko Adhi	Department Head/ PhD	Research Center for Electronics and Telecommunication, Indonesian Institute of Sciences (LIPI), Indonesia	purwoko.adhi@lipi.go.id
Ukrit Makong	Associate	Chaing Mai University, Thailand	



## ICT Virtual Organization of ASEAN Institutes and NICT (ASEAN IVO)

---

	Professor/PhD		
Nguyen Tan Hung	Associate Professor/PhD	Danang University of Technology and Science, The Danang University	
Naokatsu Yamamoto	Director/PhD	National Institute of Information and Communication Technology (NICT), Japan	naokatsu@nict.go.jp
Mitsuji Matsumoto	Emeritus Professor/PhD	Waseda University, Japan	mmatsumoto@waseda.jp

## **IV. Project Report**

### **i) Introduction**

With the increasing popularity of multimedia services supplied over the cellular radio frequency networks, including data services such as web browsing, audio and video on demand, it is certainly only a matter of time before users will face extreme congestion. Advances in displays, battery technology and processing power have made it possible for users to afford and carry around smart phones and tablets. Hence, as we are entering a new era of always-on connectivity, the expectation from users for not only ubiquitous, but also seamless voice and video services presents a significant challenge for today's communication systems. The prospects for the delivery of such multimedia services to these users are crucially dependent on the development of low-cost physical layer delivery mechanisms. It is recognized that the electromagnetic spectrum has become extremely crowded. In addition, Internet of Things is becoming a hot topic. Transmitting a vast amount of data between connected devices will become increasingly difficult using radio-wave alone. A new potential transmission method should be explored and thoroughly developed for future sustainable communications.

This project has developed important technologies using visible light communications that can be useful in the future Internet of things, sensing, and high-speed communications. The developed technologies in this project can be categorized into six sub-topics, including: (1) visible light communication for internet of things; (2) secured visible light communications; (3) indoor localization; (4) networking; (5) ultra-high-speed indoor communication; and (6) sensing system using non-invasive optical sensors. In each subcategory, new system concepts, system prototypes, and proof-of-concept demonstrations were proposed and successfully implemented. Several pioneering efforts with significant results have been demonstrated, including: (i) a first end-to-end smartphone visible light communication system; (ii) a highest spectral efficiency organic light-emitting diode based visible light communication; (iii) a first cascaded optical wireless and millimetre-wave system for high-speed indoor communications. Furthermore, we demonstrated successfully an ultra-high-speed optical wireless communication system using advanced technologies with an achieved data rate of 100 Gb/s. Pioneering research efforts have also been made in the fields of networking and secured visible light communications using quantum key distribution and multiple-input and multiple-output technologies.

Looking into the future, the need for more bits, more spectrum, and higher network densification to support unprecedented demands for new services, such as haptic communication, high-fidelity virtual and augmented realities, virtual meeting rooms, networked games, and smart health care, require the wireless network to provide at least Terabits/second aggregated bit rate in small regions. Among the potential technologies, we believe that visible light and infrared spectrum will play a vital role. Based on the achievements in this project, we will further explore new solutions and applications to facilitate a future smart society and support the 2030 Agenda for sustainable development by the United Nations.

## **ii) Project Activities**

### **(1) Development and Implement**

In this project, several technologies and application based on visible light and infrared spectrums have been developed. Details of the developed technologies are summarized as follows,

#### **A. Visible light communication technologies for IoT applications**

##### **A.1. Mobile Visible Light Communication**

###### **Introduction**

In this work, we present the design and implementation of an end-to-end mobile screen-to-camera visible light communications system, where the transmitter (Tx) and the receiver (Rx) are both embedded in personal devices such as smartphones and tablets. In the proposed system, the transmitted data is encoded into images and subsequently beamed out on the Tx flashing screen. Once these images are captured at the receiving end, a frame subtraction is performed to recover the originally transmitted data. A Canny edge detector is utilized, and the corners of the Tx are identified on the received frames so that a perspective transformation can be applied to reconstruct the originally transmitted data and recover it. Two modulation schemes are tested, including On-Off-Keying (OOK) and Colour-Shift-Keying (CSK). The system is practically implemented and demonstrated on different Android mobile devices and a range of experiments are carried out to test and evaluate the effect of different mobility parameters system's performance including the communications link distance (between the Tx and the Rx), the Tx movement within the Rx's camera's receiving field of view, as well as the Tx rotation and tilting angles. The developed mobile VLC system's capacity used in this scheme is 5.8 kb/frame. In order to enhance the system's portability and simplify the detection process, a new detection method is developed. Firstly, the data is encoded into coloured cells and displayed on the Tx's flashing screen followed by a frame subtraction to locate the Tx on the received frames. Two modulation schemes are implemented and compared using several mobility metrics. The remaining steps are practically implemented in an Android device for a full experimental evaluation.

The proposed system offers inherent advantages in terms of portability and simplicity of implementation as it uses available screens and cameras. Additionally, the system is software based and it does not require any hardware modifications on the devices, thus making a high potential for millions of consumers. The proposed camera VLC system is also designed for the transmission of all sorts of digital data. In fact, it converts data to a binary stream, which is then converted to coloured images that are later on displayed on the transmitting screen. Moreover, thousands of bits can be transmitted in one frame, whilst taking advantage of the current average of 25/30 fps smartphone camera rate. It would be very useful in exchanging data such as coupons, brochures or maps in public spaces, where the lack of privacy and security is prominent. Additionally, the system was implemented and tested on different devices, to confirm its testability and feasibility on different platforms.

###### **System description**

Figure 1 shows a typical screen to camera VLC system, adapted to smartphones. The Tx transmits the cells representing data by displaying them on the screen. The Rx uses its

camera to capture the data and recover it. It is worth noting that a cell is a group of similarly-coloured pixels representing a single data bit when using OOK or 3 data bits when using CSK. Figure 2(a) depicts the functional block diagram of the proposed system. The transmitter converts the input data into a binary stream using ASCII coding scheme where each single bit in the stream is then converted to a cell, black or white depending on its value as 0 or 1, respectively. An image is then created and displayed on the flashing screen of the transmitting phone. On the receiving side, the smartphone's camera acquires the displayed frames. The Tx is then detected on the captured frames, before data recovery. The most important steps in this functional block diagram are the image display on the device's flashing screen and the detection of the received frames. They are both highlighted in Fig. 2(a). Further details regarding these two steps are given in the following sections.

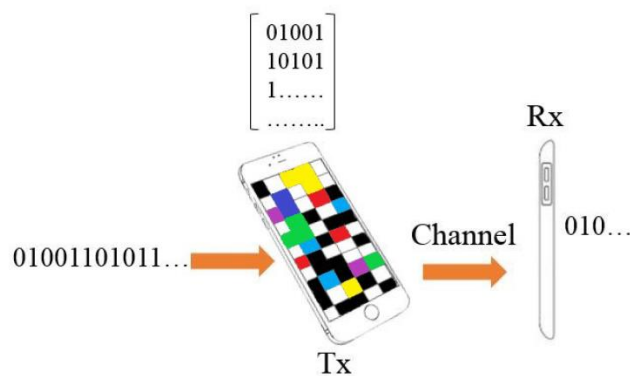


Fig. 1: A typical screen to camera VLC system.

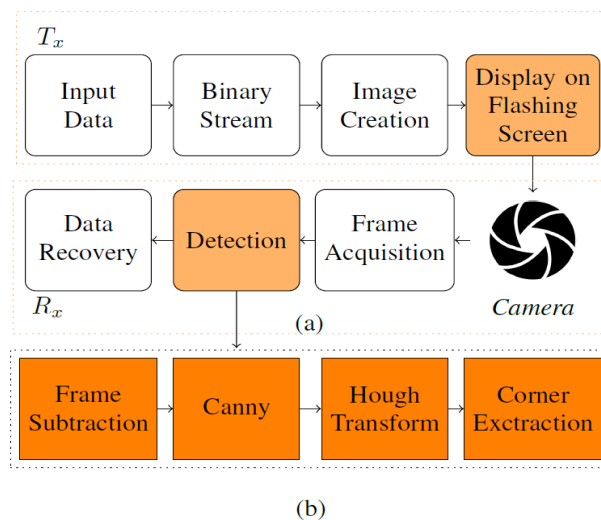


Fig. 2: Mobile VLC system block diagram.

*- Data modulation and image creation*

The Tx converts the input data into a binary stream using ASCII coding scheme. The binary stream is then modulated using OOK or CSK.

- OOK: Although this is not the most efficient modulation scheme in terms of data throughput, it is widely used in VLC for simplicity purposes, especially in the development and testing phases of a new system, which was the case in this scheme. The OOK symbols are replaced

by cells. Applying OOK in this case means using solely two colours on the display: black (for 0) and white (for 1).

- CSK: CSK modulation can be applied to S2SVLC by transmitting red/green/blue images containing coloured cells, where the colour of each cell can be encoded into 3 bits, which increases the potentially achievable system's throughput. In order to create a transferable image with coloured cells, three binary streams are converted to three bi-dimensional images, which are superposed to form the final RGB image displayed on the Tx. They represent its red, green and blue components. Each cell in this case represents three bits (8 different colours) instead of one. The image displayed on a flashing screen, similarly to the black and white case. The detection also remains the same.

*- Display on flashing screen*

The input data is converted into a binary stream. In order to facilitate the detection on the receiving side, the transmitter's screen flashes. This is achieved by making the screens brightness toggle between a high level of brightness for a duration and a low level of brightness for another duration of time.

*- Transmitter's detection*

In the detection step, high precision is necessary as the system's accuracy of the recovered data depends on it, essentially. Figure 2(b) represents the detection block diagram. Following the image acquisition, a subtraction is performed between every two consecutive frames. If two consecutive frames represent a dark frame and a bright frame respectively, the remaining detection steps will be executed by the receiving mobile device. Firstly, a Canny edge operator is applied, followed by a Hough transform, in order to detect the transmitters edges. A simple line intersection calculation allows the determination of the four corners of the Tx. These corners are then used to reconstruct the distorted Tx.

*- Bit extraction*

The order in which the lines and corners are extracted is unpredictable and depends essentially on the detected lines strength. Therefore, data extraction requires an additional step in order to determine the starting point of the extraction. The proposed system is designed to adapt to high mobility including rotations around the three axes. Therefore, when the captured screen is reconstructed, it can be in any one of the four directions represented in Fig. 3. Hence, a specific marker known by both sides of the communication link is added to the displayed frame on the transmitting side. Unlike the QR code extraction technique and Cobra detection method, the marker is only used after the Tx detection and corner extraction, to help with the recovery of the transmitted bits.

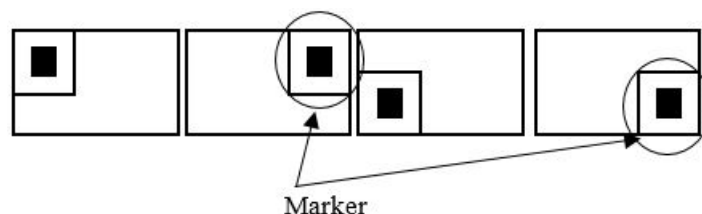


Fig. 3: Different marker positions.

### Experimental demonstration

#### - Hardware implementation

Three scenarios were investigated in order to evaluate the system's performance in a dynamic environment. In the first scenario (which is also the most promising case) all the transmitted frames are different, and they are updated at the camera rate. In the second scenario, the data displayed on the transmitting screen is updated every time the screen flashes. In other words, a dark frame  $F_D$  is displayed followed by  $n$  number similar bright frames. Then, another dark frame  $F_D$  is displayed followed by a new bright frame. Both cases 1 and 2 require a screen refreshing time to update the data displayed on the screen. Given that this parameter is not considered in this scheme as the investigation will focus mainly on the post-processing operated by the Rx, the simplest case was implemented on the Tx, where all the transmitted frames  $F_n$  are identical. Several parameters, presented in Fig. 4, were investigated in order to evaluate the system's performance. These parameters include the distance  $d$  between the Tx and the Rx, the rotation angle  $\theta$ , the tilting angle  $\alpha$  as well as the Tx's translation within the Rx FOV. Table I represents the parameters used in the experimental work. Whilst displaying the data frame, the application also makes the screen flash, by increasing and decreasing the screen's brightness constantly. The flashing screen requires a rise time when it flashes between low brightness and high brightness on the Tx. The screen rise time is measured using a photodiode when BH= 50% of the maximum brightness. The duration of the dark frame was also investigated, and the optimal parameters are used in the work presented here. The cell size used in this scheme is also presented in the table. The cell area is given in  $\text{mm}^2$  as the number of pixels in one cell has no effect on the system whereas the cell size does.

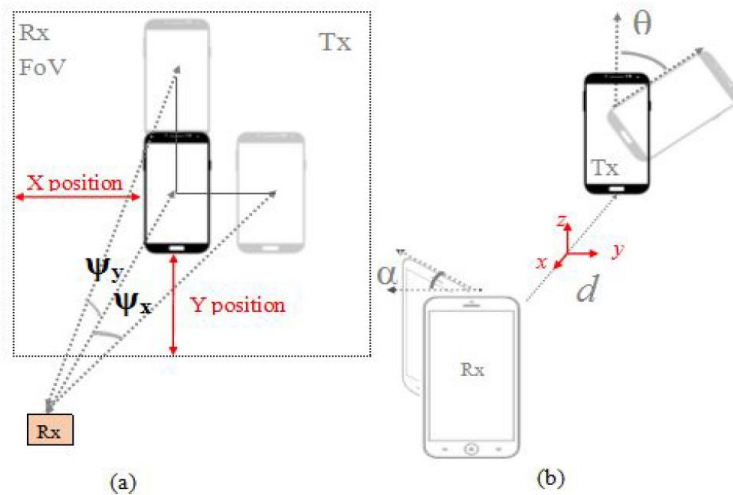


Fig. 4: Investigated parameters.

TABLE I: Experimental parameters

	<b>Parameter</b>	<b>Value</b>
Channel configuration	Distance ( $d$ )	12 cm to 51 cm
	Rotation angle $\theta$	0° to 180°
	Tilting angle $\alpha$	-90° to 90°
Tx OOK	Device	1280x720 (Samsung Galaxy SIII)
	$B_L$	200 ms
	$B_H$	800 ms
Rx OOK	Device	13 Megapixel (LG G3)
	Data rate	2048 bit/frame
	Cell size	2.8 mm <sup>2</sup>
Tx CSK	Device	2048 x 1536 (Samsung Galaxy Tab S2)
	$B_L$	200 ms
	$B_H$	800 ms
Rx CSK	Device	8 Megapixel (Samsung Galaxy Tab S2)
	Data rate	5814 bit/frame
	Cell size	10.3 mm <sup>2</sup>

*- Software development*

The system is implemented on Android platform. On the Tx, a mobile application was developed where the user can enter a text to transmit it. The text is then converted to a binary stream, and then modulated using OOK or CSK (black and white or coloured cells respectively). A bitmap is then formed using the cells and is displayed on the Tx screen. A mobile application is developed where the user can start and stop capturing frames. The received frames are then processed one by one, where the Tx's location is updated every time a dark frame is received. Table II outlines information about the software development.

TABLE II: Software development information

<b>Parameter</b>	<b>Value</b>
Tx OOK OS version	Android Jelly Bean 4.3.x (API 18)
Rx OOK OS version	Android Marshmallow 6.0 (API 23)
Tx CSK OS version	Android Jelly Bean 4.3.x (API 23)
Rx CSK OS version	Android Marshmallow 6.0 (API 23)
Graphic library	Open CV 2.4
Integrated Developing environment	Android studio 1.2.1 and

**Results and Discussion**

The system is evaluated using the Bit Success Rate (BSR) metric which represents the percentage of successfully recovered cells. The first parameter to be investigated is the effect of the distance  $d$  (see Fig. 4) between the Tx and the Rx on the system's performance. The other experimental parameters were fixed throughout the distance range ( $\theta = 0^\circ$ ,  $\alpha = 0^\circ$ ) while  $d$  varies. The initial distance value is  $d = 12$  cm when testing OOK and  $d = 20$  cm for CSK (depends on the Tx size). Figure 5 shows the BSR against the distance  $d$ . For OOK, within the range [12 cm, 34 cm] the BSR is highly promising as it remains between 93 and 100%. In the range [34 cm, 45 cm], the BSR drops below 90% but remains reasonable as above 80%. The experiment final distance investigated was 52cm as the BSR drops below 80% and is no longer acceptable, given that the transmitted cells are either black or white, and two different images can present a BSR of 50%. However, the BSR obtained using CSK

modulation is only satisfactory within the range 20 to 40 cm, which was the last distance tested, as the BSR drops below 80%. This result is expected as the inter-symbol interference effect is more important when the cells are coloured, as it becomes harder to distinguish the different bright colours (white, yellow and cyan).

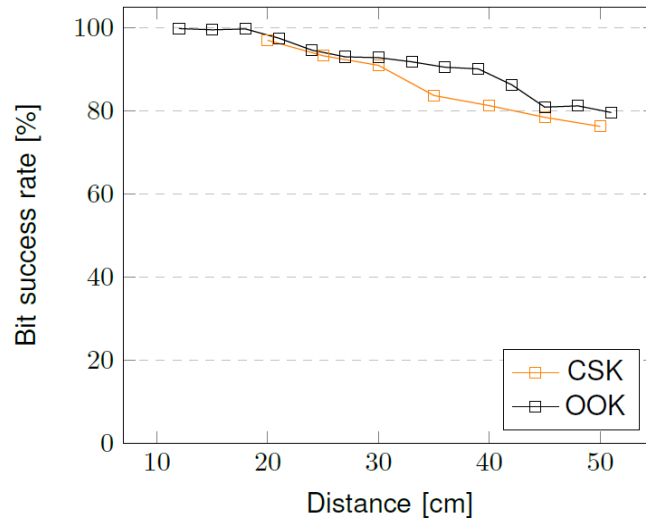


Fig. 5: System performance against distance.

The second experiment is the Tx translation within the Rx field of view (FOV). The FOV was sampled into a number of X and Y positions. Again, the only parameter that varies is the position of the Tx within the Rx FOV. The other parameters remain constant throughout the experiment. The Tx X position varies between 10 and 85% of the FOV width, and the Y position varies between 10 and 85% of the FOV height. Although the higher BSR was obtained at distances lower than  $d = 28$  cm, this distance allowed the FOV to obtain more samples from the FOV, thus evaluating more positions. The results are presented in Fig. 6. The BSR remains relatively flat as it varies between 90 and 96% data recovery, demonstrating that the system performance is invariant to the Tx translation within the Rx FOV, using either OOK or CSK modulations.

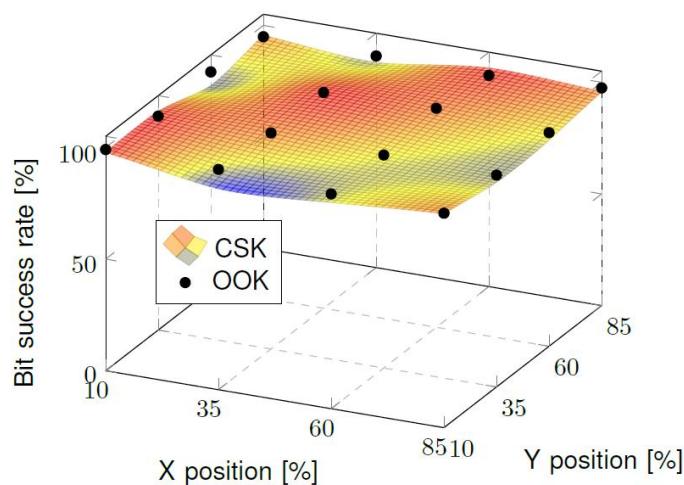


Fig. 6: System performance against translation.

The next experiment is related to the rotation angle  $\theta$ . Both the Tx and the Rx are in a parallel position, but the Tx is rotated around the z-axis, see Fig. 4. The angle  $\theta$  is varied within the range  $[0^\circ, 180^\circ]$ , whilst the other parameters are fixed. The results are depicted in Fig. 7. Once again, the BSR remains reasonably stable and reaches up to 100% data recovery using either OOK or CSK, showing that the system is robust to parallel rotation.

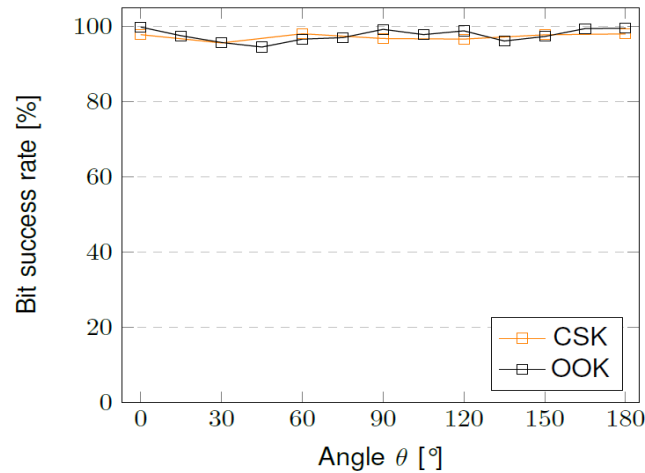


Fig. 7: System performance against rotation.

Another geometric experiment is carried out, investigating the effect of the tilting angle  $\alpha$  on the system performance as shown in Fig. 8. The angle  $\alpha$  is varied within the range  $[-60^\circ, 60^\circ]$  whilst the other parameters remain the same throughout the data collection. The results are depicted in The BSR obtained when  $\alpha$  varies between  $-30^\circ$  and  $+30^\circ$  are fairly high and above 95% data recovery. However, outside the  $[-30^\circ, 30^\circ]$  range, the BSR decreases dramatically to 80% at  $-45$  and  $+45^\circ$ , and below 50% at  $-60$  and  $+60^\circ$ . Once again, similar results are obtained for OOK and CSK.

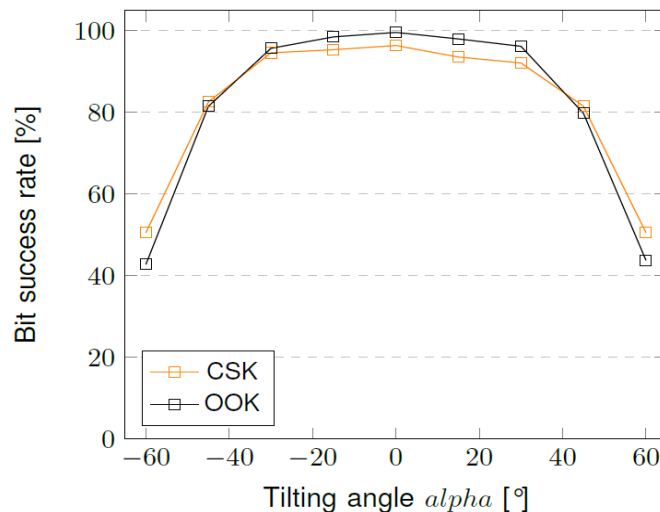


Fig. 8: System performance against tilting.

## **Conclusion**

The system was evaluated, and the obtained results showed good outputs. In fact, different mobility conditions such as the link distance between the Tx and the Rx, rotations of both the Tx and the Rx devices were included to characterize the system under normal use. Practically, S2SVLC offers a range of new features with a 90° field of view and a reasonable distance range for short range communications (12 to 51 cm using OOK and 20 to 40 cm using CSK). Additionally, the flashing screen facilitates the portability compared to the previous work in [12] where a detection frame was needed, and the algorithm could be combined with standard compression techniques and error correction, for data rate enhancement. The investigation has demonstrated a promising system for a short-range smartphone to smartphone communication. The comparison of OOK and CSK also showed that although CSK is superior in terms of data throughput, OOK's performance remains better over longer distances, and RGB images take longer to process. Moreover, this work provides a full implementation of the system to different terminals/devices than smartphones, widening thus its applications. It also offers a technology easier to implement as it relies on the flashing screen, rather than on a pre-learned header that needs to be known in advance from both sides of the communication. Moreover, the system offers a channel capacity of more than 2 kb/frame using OOK and 5.8 kb/frame using CSK. However, with newer processors and higher resolution cameras, hundreds of kilobits per second can be transferred using this technology. Although CSK presents a higher potential as each cell transmits three bits compared to one bit for OOK, the inter-symbol interference effect is more important for CSK as colours can be similar depending the communication conditions, and the processing time is higher considering the size of the received images.

## **A.2. Organic Light Emitting Diodes based communications**

### **Introduction**

In visible light communication (VLC), visible light sources are used as transmitter to support wireless data transmission. The approach has been considered as a promising solution for 5G wireless networks, especially for indoor communications. Recently, multi-gigabit per second transmission link has been demonstrated using light emitting diodes (LED). However, LED is not as good as its alternative organic LED (OLED) in terms luminous efficiency and power efficiency. With advances in research and development, production price of OLED has been reduced and commercial OLED panels are now available. One of the most challenging problems in a VLC system is the narrow modulation bandwidth of the light source. Various techniques have been investigated to enhance data rate such as equalizer, multiplexing and multi-level modulation. The illumination area of commercial OLED is usually larger than that of LED. As a result, the increased equivalent capacitance greatly increases the transient response and further decreases the modulation bandwidth.

Report on VLC system with OLED focused on passive pre-equalizer at the transmitting side in combination with non-linear post-equalizer at the receiving side. Passive pre-equalizer using bias-tee enhanced the modulation bandwidth by less than 10 times but caused baseline wander and reduced luminous flux. Non-linear discrete post-equalizers using artificial neural network and multilayer perceptron artificial neural network were very complex to implement on real-time system. On the other hand, different modulation methods have been applied to

VLC system with OLED. Generally, non-return-to-zero (NRZ) scheme provided better bandwidth efficiency than multicarrier modulation schemes such as discrete multitone and OFDM. However, to the best of our knowledge, no direct comparison of amplitude and multicarrier schemes in the same system has been reported. For off-line system, the state-of-the-art system used NRZ with transmission distance of 10 cm. For real-time system, the farthest transmission distance was 40 cm and was also achieved with 2-level amplitude modulation. The reasons were that: (i) Modulated light can only support non-negative real values; (ii) Incoherent light sources only support amplitude modulation/detection; (iii) Usable bandwidths assume low-pass filter shape. Thus, modifications have to be made to convert the complex values of multi-carrier modulation schemes to nonnegative real values, resulting in the usage of lower subcarriers and symbols. The high signal-to-noise ratio (SNR) sub-carriers near DC region were also poorly utilized.

In this subsection, we proposed a new combination of active pre-equalizer and Filter Bank Multi-Carrier (FBMC) modulation for VLC system with OLED. Instead of reducing low signal frequencies gain using a bias-tee, we amplify the high signal frequency gain using a band-pass amplifier. Instead of using OFDM, we apply FBMC to utilize the high SNR sub-carriers near DC region. As a result, our proposed system has achieved a bandwidth efficiency of 286 bps/Hz, which was 5 times higher than the state-of-the-art system. Moreover, we have also compared and analyzed performance of NRZ, OFDM and FBMC in our system. The results indicated that FBMC supports better aggregate bit rate for short distance transmission while NRZ is more robust at long distance transmission.

#### **Development of Pre-Emphasis Circuit for OLED**

To the best of our knowledge, reported VLC systems with OLEDs still lack the required range and data rate to replace Wi-Fi systems for indoor wireless communications. Thus, our proposed VLC system was investigated for other applications such as indoor localization, sensor networks, internet-of-things. Commonly used protocols for such applications are Bluetooth, near-field-communications and ZigBee. Required data rate is around several hundred kilobits per second. Our VLC system is shown in Fig. 9. At the transmitting side, Tx signal voltage and current follow TTL protocol for easy integration with available electronic systems. The proposed driving circuit is sandwiched between the input port and the OLED light source. The driving circuit consists of an active equalizer and a power amplifier. The active equalizer or pre-emphasis circuit compensates for the limited modulation bandwidth of the OLED while the power amplifier provides enough power to drive the OLED. At the receiving side, a free space visible light photodetector with trans-impedance amplifier (TIA) is used to detect and convert light signal into electrical signal. Optionally, a comparator can be used after the TIA as in our previous system [8] for 2-level amplitude modulated signals. The Rx signal can be connected to any ADC with 50 impedance matching for further processing.

Generally, the OLEDs structure and material determine its frequency response. In [9], temporal response of OLED was simulated using various physical parameter such as carrier mobility, exciton lifetime, energy level offset, bias voltage and devices length. In another report [10], the frequency response of OLED was estimated using charge carrier injection properties of different anodes and anode treatments. Equivalent circuit model of OLED was also reported in [11]. Basically, the OLED frequency response can be considered as a low-pass filter circuit. However, its equivalent capacitance changes with frequency.

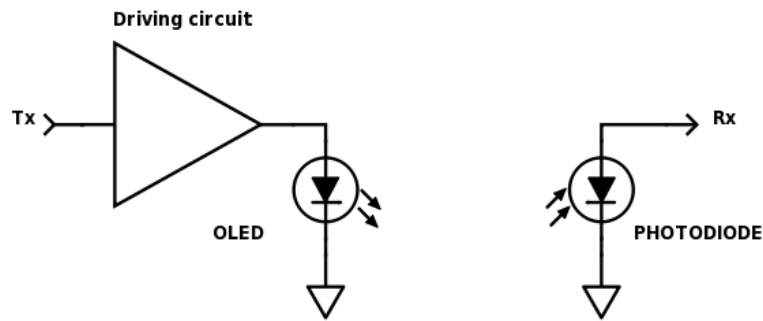


Fig. 9. Block diagram of the proposed OLED-based VLC system.

To compensate for the measured OLED frequency response, we proposed a driving circuit consisting of an active equalizer and a power amplifier as shown in Fig. 10. The active equalizer compensated for the limited modulation bandwidth of the OLED while the power amplifier provided enough power to drive the OLED. For the active equalizer, a modified active band-pass filter circuit using operational amplifier (TL082) was designed with the following transfer function:

$$H_{pre}(f) = \frac{R_3}{R_2} \cdot \frac{1}{1 + j2\pi f C_2 R_3} \cdot \frac{1 + j2\pi C_1 (R_1 + R_2)}{1 + j2\pi f C_1 R_1}$$

By modifying the values of the electronic components, the band-pass amplifier could provide more power at higher frequency without distorting lower frequency bands. The measurement results in the previous section were used to find the most suitable values for the electronic components of the active equalizer. For the band-pass amplifier, the components were selected by both simulations using Protues and measurements in our laboratory. As shown in Fig. 11, simulated and measured results were closely matched up to 500 kHz. The circuit was intended to compensate for the frequency range from DC to 100 kHz only. A more sophisticated circuit to compensate for both the gentle slope around 100 kHz and steep slope around 1 MHz is still being investigated. For the power amplifier, the OLED driving voltage and current are 8 V and 250 mA, respectively. In our design, the amplifier circuit using power MOSFET (IRF3205) provided driving voltage and current of 7 V and 220 mA, respectively. The slightly reduced power was for safety margin during operation. As shown in Fig. 11, the power circuit further increased the 3-dB bandwidth to 320 kHz. As a result, the modulation bandwidth of our OLED-based VLC system was expanded more than 45 times, from 7 kHz to 320 kHz. To the best of our knowledge, modulation bandwidth of reported OLED based VLC systems can only be expanded less than 6 times using other methods. Moreover, our proposed driving circuit could mitigate several issues persisted in other published methods. Driving circuits using bias-tees cause substantial attenuation at DC and low frequency components. Driving circuits using high impedance NAND gates only support on-off-keying modulation method. In the experiments, our proposed circuit supported multi-level modulation methods and increased SNR for higher frequencies without any compromise at lower frequencies. Additionally, by utilizing a commercial off-the-shelf OLED, the experimental results in our report could provide complementary and insightful information to other reports using fabricated OLEDs. Firstly, fabricated OLEDs are extremely small in size. The largest one has an illumination area of only 9 mm<sup>2</sup>. For lighting and display

purposes, commercial OLEDs are usually much larger in size. Typically, off-the-shelf OLEDs products from companies such as Osram and Phillips have an illumination area larger than 5000 mm<sup>2</sup>. In turn, the larger size increases the equivalent capacitance between organic layers, which strongly affects the frequency response. Secondly, fabricate OLEDs are optimized for single color radiation, while off-the-shelf OLEDs are designed to imitate white light. The different in structure can significantly change the frequency response. As a result, the optimized drivers for fabricate OLEDs may not be the best one for commercial OLEDs.

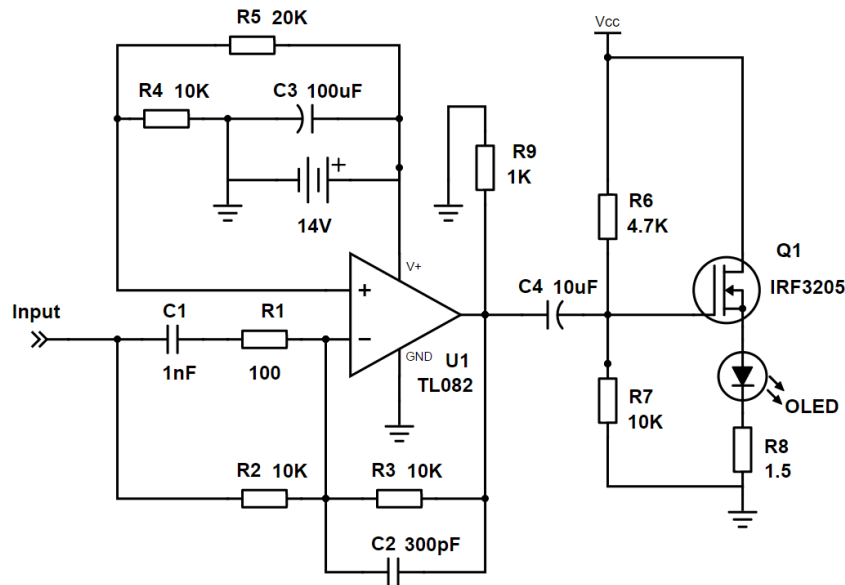


Fig. 10. Driving circuit for an OLED.

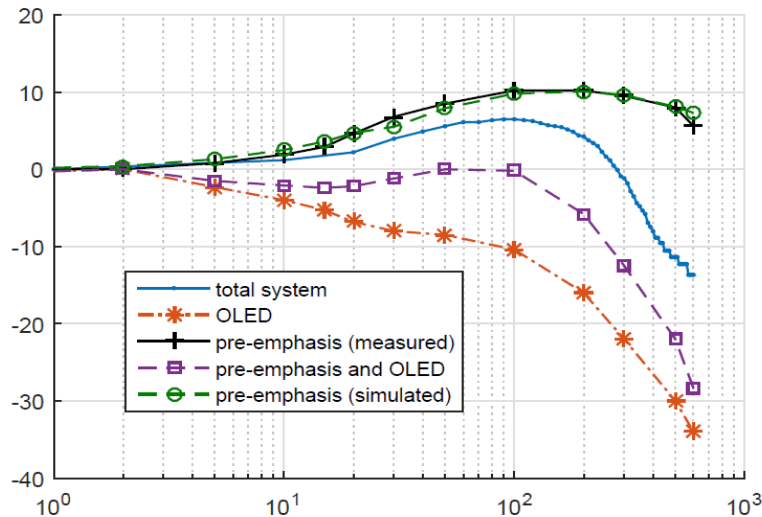


Fig. 11. Systems frequency response.

### Modulation Methods for OLED

Modulation schemes for VLC system with LED can be classified into two board categories: amplitude modulation and multicarrier modulation. For comparison purposes, we have tested our system with amplitude modulation (NRZ) and two multicarrier modulations, namely,

OFDM and FBMC. To the best of our knowledge, even though FBMC has already been investigated for VLC, this is the first time FBMC signal was used for VLC system with OLED.

- NRZ: For this simple modulation scheme, the input signal was a 2-level amplitude modulation signal. From the frequency response of the system, it is expected that the modulated signal would suffer from over-shoot pulses caused by the over-compensate gain at higher frequencies.
- OFDM: OFDM is a multicarrier modulation scheme where the transmitted bits are modulated and multiplexed on different subcarriers. Simplified block diagram of a typical OFDM system is depicted in Fig. 12. Generally, the transmitted symbols are firstly converted from serial to parallel. Then, IFFT is performed on the symbols at M subcarriers to achieve frequency orthogonality. After the parallel-to-serial (P/S) conversion process, a cyclic prefix (CP) is appended to each OFDM symbol. The CP is introduced in order to reduce inter-symbol interferences, inter-channel interferences and simplify the channel equalization. However, the CP does not carry any information and induces a loss of throughput. At the receiver side, reciprocal operations are performed, i.e., removal of the CP, S/P conversion, FFT, channel equalization and finally P/S conversion. OFDM has several advantages. Firstly, the CP reduces channel equalization complexity, which sums up to a simple per-subcarrier scalar multiplication after the FFT at the receiver. Secondly, subcarrier interleaving increases resistance to frequency-selective channel conditions such as fading and attenuation. Particularly, for indoor VLC, the channel is line-of-sight dominant with slow Rayleigh fading. Thus, the frequency response as in Fig. 11 indicates that signal-to-noise ratio (SNR) will varies at each subcarrier. Therefore, the number of transmitted bits on each subcarrier can be optimized based on its SNR and target error probability. It should be noted that OFDM signals have complex values and cannot be directly modulated with light, which supports only non-negative real values. Moreover, the inherently incoherence light of OLED is only suitable for amplitude modulation and detection. In our proposed system, a modified DC-bias OFDM approach is used. The complex baseband signal is digitally upconverted to a central frequency making it real with spectrum conjugate symmetry. Then, DC offset is added to remove negative values. A guard band has to be inserted to avoid interference between the DC frequency and the signal spectrum.

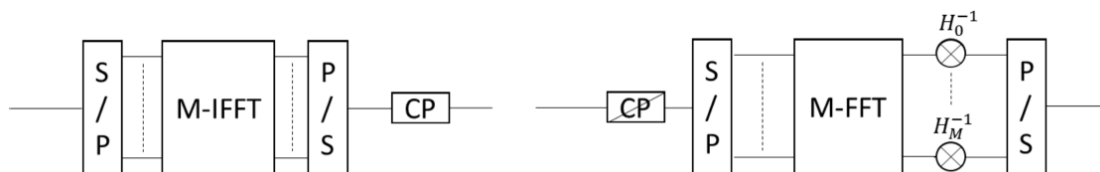


Fig. 12. Block diagram of OFDM modulation and demodulation. The abbreviations S/P, P/S, (I)FFT and CP stand for serial-to-parallel, parallel-to-serial, (inverse) Fast Fourier transform and cyclic prefix respectively.

- FBMC: Similar to OFDM, FBMC is a multicarrier modulation utilizing frequency orthogonality. However, FBMC has two major advantages in comparison with OFDM. Firstly, as shown in Fig. 13, a polyphase network (PPN) is added after IFFT at the transmitter and before FFT at the receiver. The PPN implements additional filtering in time domain and drastically reduces spectral leakage of the modulated pulses at each subcarrier. As shown in Fig.14, the FBMC

signals spectrum can be much closer to the carrier tone than OFDM signals spectrum without any interference. Secondly, since the pulse shape is much more frequency selective, channel equalization for FBMC can be performed without CP. Thus, FBMC supports higher spectral efficiency than OFDM. To the best of our knowledge, FBMC has never been proposed for VLC system with OLED. Given the frequency response as in Fig. 11, the best modulated spectrum should be from DC to around 320 kHz. Since FBMC does not require a guard band near DC in comparison with OFDM, it would be able to utilize the low frequency sub-carrier and achieve a higher overall SNR. Since FBMC signals also have complex values, the same approach described in the OFDM section is applied. Firstly, the FBMC signal is upconverted to a central frequency. Then, a DC offset is added to generate non-negative real values.

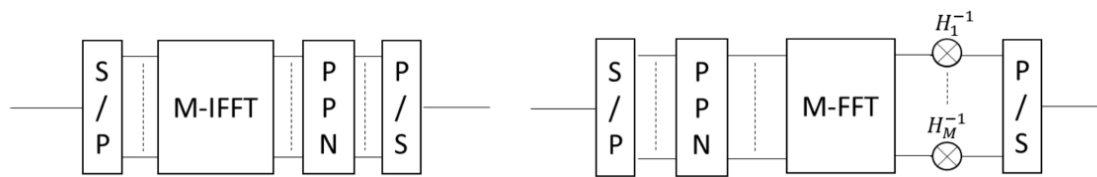


Fig. 13. Block diagram of FBMC modulation and demodulation. The abbreviation PPN stands for polyphase network.

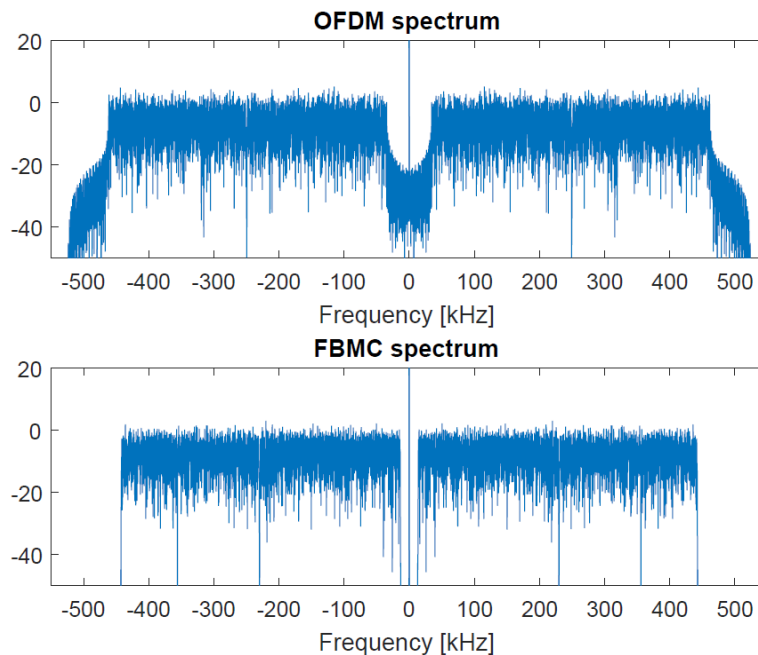


Fig. 14. OFDM and FBMC spectrum.

### Experimental setups for data transmission

A set-up similar to Fig. 9 was used to test the systems performance. The transmitted signals, generated in Matlab, were used as input waveform for an arbitrary function generator (AFG Tektronix AFG3011C). The transmitted electrical signal (Tx) current was 40 mA and voltage varied from 0.8 V to 3.2 V. Both the OLED and PIN were aligned and fixed on an optical table. During the experiments, ceiling lights were turned off to minimize ambient noise. A lower

gain increased the TIAs bandwidth. However, SNR was also reduced. In the end, the PIN TIAs gain was set at 30 dB and its 3-dB gain bandwidth was 260 kHz. The received electrical signals (Rx) were captured on an oscilloscope (Agilent DSO-X4104A). Finally, de-multiplexing of Rx was performed off-line in Matlab. In our system, Phillips Lumiblade OLED was used. Its optical spectrum had a peak at 606.308 nm and the most prominent shoulder at 525.213 nm. Its 3-dB modulation bandwidth was 7 kHz. A Thorlab PDA36A Si PIN was used.

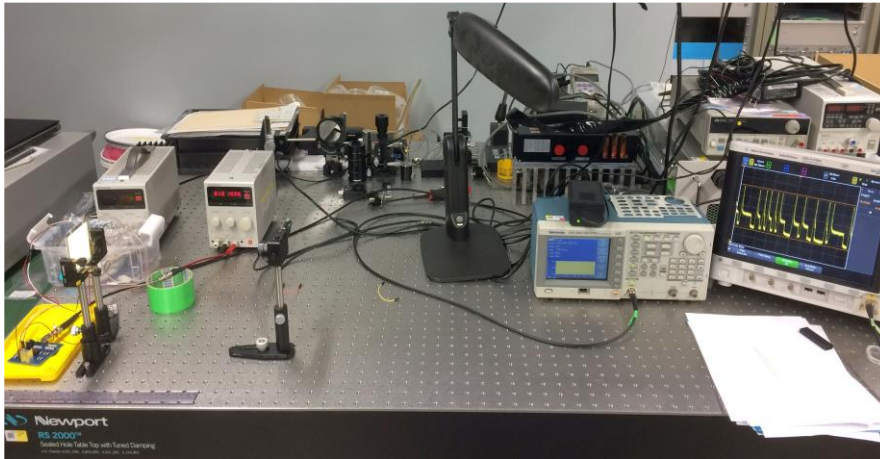


Fig. 15. Photo of the experimental set-up.

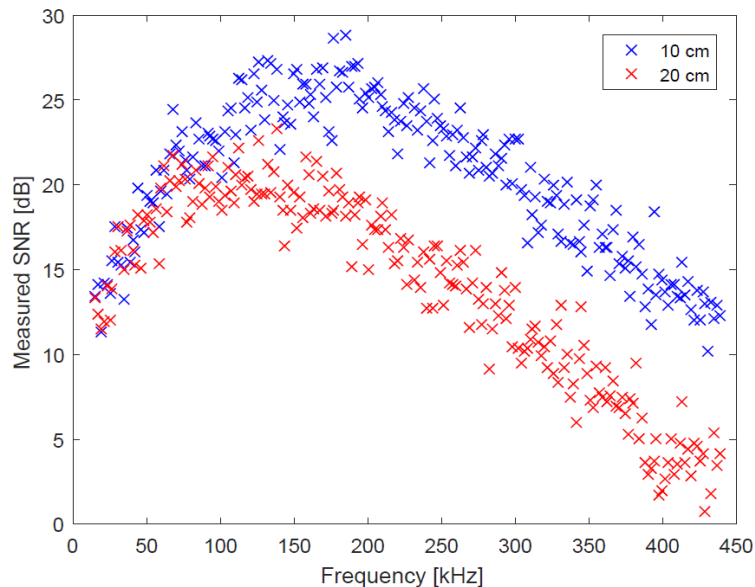


Fig. 16. Per-subcarrier measured SNR of the FBMC signal for two different distances.

In our experiments, NRZ signals were simply two-level amplitude modulation signals. For OFDM signals, the number of subcarriers was 256. The sampling frequency was 500 kHz. Out of 256 subcarriers, the DC and 19 other subcarriers at the edges of the band were left inactive, which led to a signal bandwidth of 426 kHz. The central frequency for OFDM was 250 kHz. CP length was fixed to one fourth of the OFDM symbol, i.e., 64 samples. For FBMC, the same number of subcarriers and sampling frequency values were used. However, since there was no guard band, the center frequency for FBMC was 230 kHz. No CP was needed for FBMC signal. Basically, the signal spectra were similar to Fig. 14. Measured SNR for all

sub-carriers of the FBMC signal are shown in Fig. 16. The SNR values have a shape similar to the systems frequency response in Fig. 11. These measurement results were expected as discussed in the previous section.

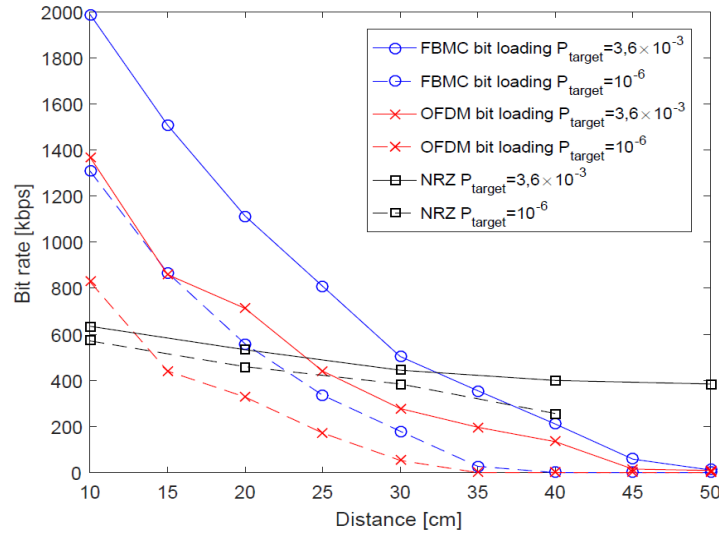


Fig. 17. Bit rate as a function of the distance for the different modulations under consideration and two target error probabilities.

Fastest possible bit rate at different transmission distances are shown in Fig. 17. The first target BER was  $3.6 \times 10^{-3}$  assuming the same forward error control method. Using FBMC at the same transmission distance, our proposed system could achieve an aggregate bit rate of 2 Mbps using a commercial OLED with 7 kHz bandwidth. Thus, we achieved a bandwidth efficiency of 286 bps/Hz. This is a significant improvement of the current state-of-the-art. Moreover, to the best of our knowledge, this is the first time the performance of amplitude and multicarrier modulation methods was directly compared for the same OLED VLC system. FBMC method supported the fastest aggregate bit rate for transmission distance up to 32 cm. OFDM method could only provide slower aggregate bit rates in comparison with FBMC. The reason was twofold: (i) OFDM method had to use CP and thus, had lower bandwidth efficiency than FBMC; (ii) OFDM method could not utilize the better SNR sub-carrier near DC region and thus, had lower SNR than FBMC. However, both multicarrier modulation methods were less resilience to low SNR than NRZ method. As shown in Fig. 17, NRZ could only achieve a data rate of 670 kbps at 10 cm. However, the bit rate only slowly degraded, and a data rate of 380 kbps could be achieved at 50 cm. Firstly, distortions caused by over-shoot could easily be compensated using a comparison threshold and bit duration synchronization. Secondly, the whole bandwidth was utilized by NRZ while only sub-carriers with adequate SNR were utilized by FBMC and OFDM. As the transmission distance increased, the number of usable sub-carriers reduced and thus the aggregate bit rate for both FBMC and OFDM was quickly degraded. For the sake of completeness, the second target BER= $10^{-6}$  without forward error control was also considered. The best aggregate bit rate was around 1.3 Mbps using FBMC at 10 cm. NRZ started to outperform both FBMC and OFDM at distances farther than 25 cm.

## **Conclusion**

We have presented a VLC using OLED system. Combining with pre-emphasis circuit and advanced modulation methods, the proposed system has been able to achieve bandwidth efficiency of 286 bps/Hz, which was five times higher than state-of-the-art reports. Moreover, experimental results indicate that different modulation schemes should be considered for different transmission distances. Multicarrier modulation schemes provided the best transmission bit rate for short transmission distances around 25-30 cm. NRZ was more robust against low SNR scenarios and more suitable for farther distances. Additionally, FBMC could utilize the subcarriers near DC and performed better than OFDM in terms of aggregate bit rate. Further researches on improving transmission distance and data rate are being investigated.

## **B. Secured Visible Light Communication**

### **B.1. Secure quantum key distribution-based VLC system**

Visible light communication using light emitting diodes (LEDs) in illumination infrastructure has been attracted a lot of scientific research interest. The main advantages of VLC are energy efficient, reliable, and eco-friendly. Besides, due to the scarce wireless resource, VLC has become a favorable complementary technology to RF communication in short-range communication scenarios for future 5G networks. Especially for 5G indoor applications, VLC has developed rapidly in the last few years. While the progress of this magnitude is intriguing, the hyper indoor connectivity that 5G networks enable will exacerbate security issues in VLC networks. Although security issues have been mentioned in several survey papers, there is still a lack of intensive studies on the issues. The IEEE 802.15.7 VLC standard also mentioned about the use of symmetric-key cryptography for improving the security of VLC networks. However, the methods of key generation and management are not detailed in the standard.

Motivated by the above discussion, we investigated an application of quantum key distribution (QKD) as a secure communication method for VLC networks. While a number of studies about QKD through optical fiber or free-space optical systems have been done so far, to the best of our knowledge, this is the first study of QKD in VLC networks. More specifically, the contributions of this work can be summarized as follows:

- Design of QKD/VLC systems: we presented the continuous variable (CV)-QKD protocol operation over a VLC link. Also, we provide guidance for the realization of CV-QKD/VLC using subcarrier intensity modulation (SIM) binary phase-shift-keying (BPSK) and dual threshold/direct-detection (DT/DD) receiver as shown in Fig. 18.

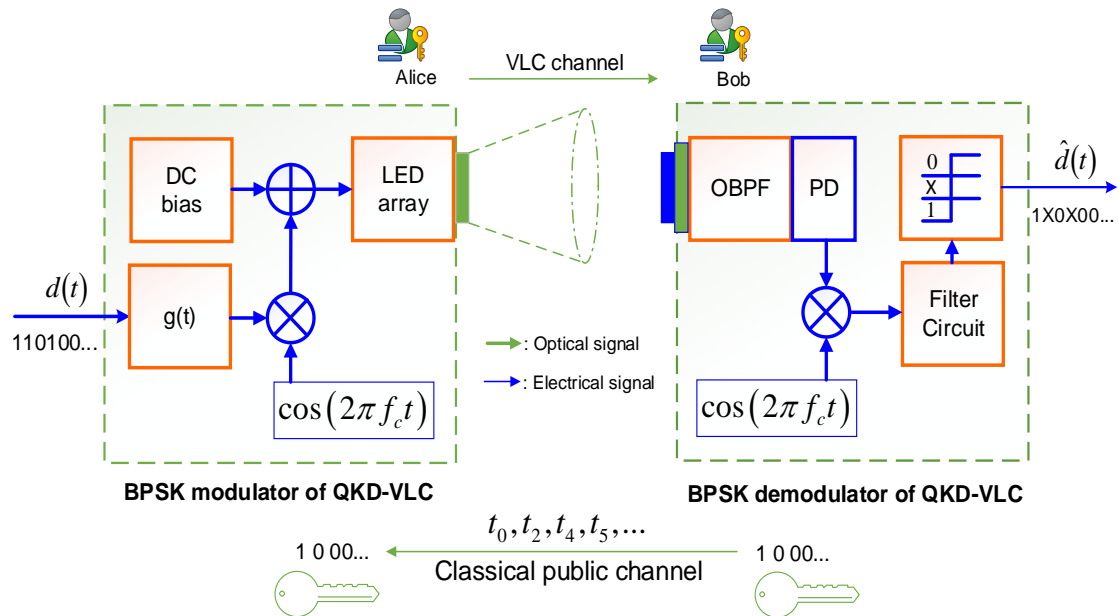


Figure 18. Block diagram of CV/QKD-VLC system.

- Performance analysis of CV-QKD/VLC systems: as the main contribution of this study, we derived mathematical expressions for quantum bit-error rate (QBER) and secret-key rate, taking into account various effects of VLC channel and system impairments. These expressions could be helpful in practice for designers to determine the system parameters. The importance is shown through selections of modulation depth and dual-threshold scale coefficient based on a design criterion of QBER and secret-key rate. Figure 19 shows an example of QBER performance for a set of typical parameters.

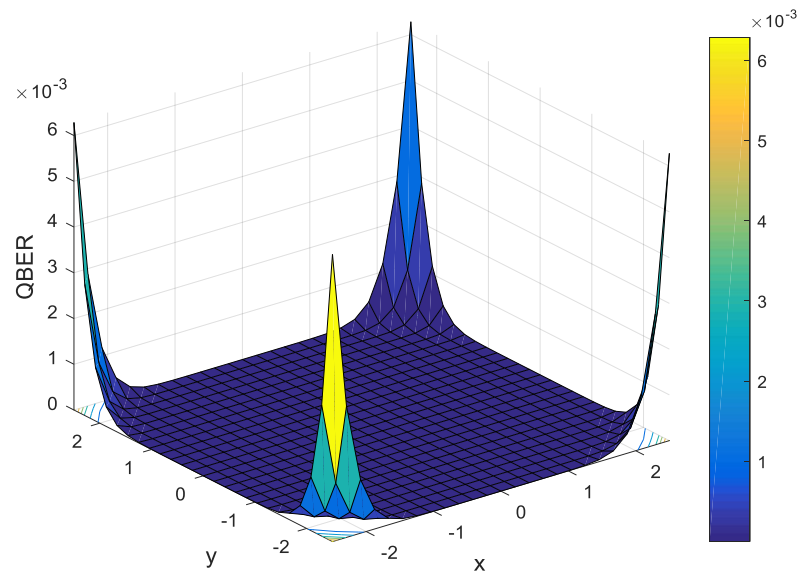


Figure 19. QBER versus different Bob's locations when the dual-threshold scale coefficient  $\delta = 1.5$ , the intensity modulation depth  $\rho = 0.25$  and PLED = -3 dBm.

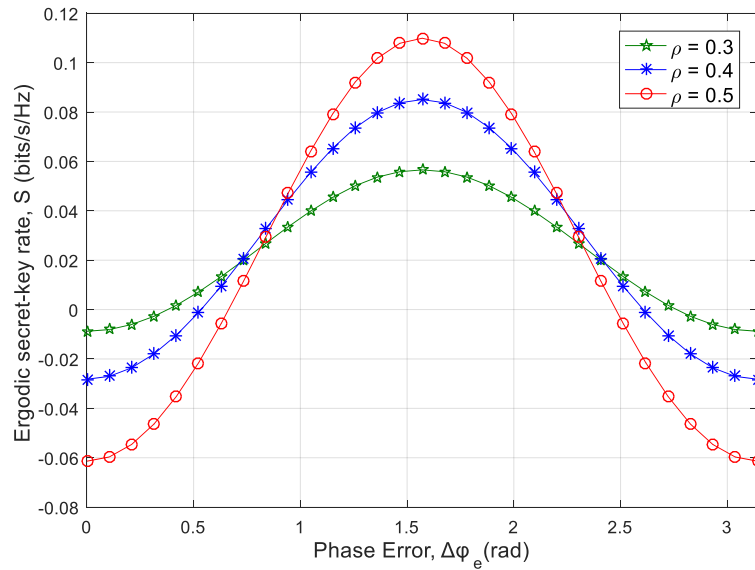


Figure 20. ESKR versus the phase error ( $\Delta\phi_e$ ) for the different intensity modulation depth ( $\rho$ ) with  $\delta = 1$ , PLED = -10 dBm,  $(x_B, y_B, z_B) = (2.0, 2.0, 2.15)$ ,  $(x_E, y_E, z_E) = (2.0, -2.0, 2.15)$ .

The numerical results also show that CV-QKD/VLC system can provide QBER that can meet the design criteria of lower than or equal to  $10^{-3}$ . In addition, it is possible to keep the system being secured, i.e., ergodic secret-key rate is larger than 0, by setting the intensity modulation depth at low level.

## C.2. Highly secured MIMO VLC

### Introduction

With the advent of solid-state LED technological progress where the LED light can be modulated at high frequencies and the greatly increased demand for high-speed wireless data communication, the emerging VLC systems have been considered as one of the promising solutions for the future of wireless network generation where the wireless carrier spectrum is increasingly higher. VLC will bring additional advantages alongside with the RF communication counterparts. Also, the integrated optics facilitate the usage of diffuse lenses along with LEDs to obtain dual luminosity and communication in VLC systems, hence, reducing the carbon dioxide emissions by maintaining energy consumptions as low as possible. The illumination intensity of LED lighting can be regulated based on the average current of the LED (DC-bias), binding it with data signal without affecting the beam profile of the LED light. VLC proves its validity to provide high data rate communication links in indoor environments, where the use of multiple-input multiple-output (MIMO) VLC systems offers a Gbps data transmission. As the light beam is concealed within the room's or office's walls, VLC potentially offers secured communication in an enclosed space. However, there is still a possibility for an eavesdropper to intercept the information within the general illumination zone as a typical VLC system provides both illumination and communication in the same beam and coverage zone. Physical-layer security, therefore, is an ingenious technique offering an effective and strong encryption method to reduce an extra computation at upper layers since it can exploit the characteristics of the physical channels to secure the information from eavesdroppers by blocking the hacker from accessing the meaningful

physical data. It also eliminates the dependency of an encryption key at the receiver where a keyless scheme was suggested to secure a VLC channel based on the wiretap channel estimation or the physical location of the receivers.

In real-life applications, a user is usually in motion from time to time therefore to achieve the physical security, it is required that the system either to provide a greater security area or to track the user position to reallocate a secure coverage for the secured VLC link. The provision of a greater area leads to the fact that there is a problem to allocate more users as well as the security might be compromised since a hacker can move its receiver next to the legitimate user. The use of the tracking system requires the transmitter to update the user location regularly, either received by the uplink feedback from the user or it needs to self-detect the user location. Obtaining a current position feedback from the receiver using the VLC uplink imposes a crucial challenge as (i) the induced irradiance of a narrow beam-width light source needs to be oriented to a fixed direction toward the receiver in the ceiling, (ii) energy limitation factor is restricting the usage of the LED to transmit information for the uplink channel, (iii) the light glare of the uplink might interfere with the downlink channel in regards to full-duplex communication producing a hindrance to human eyes in an indoor environment, and (iv) it might not be practical to have a VLC uplink due to the aesthetic point of view. Alternatively, techniques for self-determination of user location can be implemented to estimate the receiver position from the transmitter side.

In this work, we proposed a method to enhance the dynamic security of the physical layer in a MIMO VLC system using the optical tracking system. The proposed scheme provides a secure dynamic zone, which follows the receiver's position inside the illuminated zone compared with a static secured zone. By self-allocating a private physical communication channel for a user on the move, where the user position will be tracked in the transmitter side and correspondingly form an adaptive channel matrix unique to the user. Here we generate a varied scrambling matrix with respect to the unique receiver position, to form an exclusive data-recoverable zone within the original illumination area to prevent unauthorized access from receiving the original data. The main original contributions presented in this work will include (i) the development of a novel mathematical model to create a dynamic secure zone that is varied based on the receiver position within the illuminated region of a non-imaging MIMO system, (ii) the design of camera-based surveillance system integrated to the MIMO VLC transmitter to obtain self-determination of the VLC user/receiver position with different resolutions, distance and illumination conditions, and (iii) the customized utilization of image-processing techniques to obtain a high accuracy VLC user positioning system.

## **Experimental Demonstration**

### *Experimental Setup*

The proposed system is deployed, and the system block diagram is presented in Fig. 21. The experimental section covers the realization of the moving receiver, where a tracking video is introduced based on the movement of the authenticated receiver. Initially, the VLC system is simulated using MATLAB and the number of receivers and the number of transmitters are assumed to be equal for the sake of simplicity, where  $N = K = 4$ . The positioning matrix is designed for each user's new position, hence precoding the input signal, which is non-return-to-zero on-off-keying (NRZ-OOK) data. Additionally, the transmitting simulation process was performed by taking a real LED impulse response measured for each transmitter.

The NRZ transmitted signal consists of 1000 bits length. Also, the ambient noise of an indoor environment is included in the channel where an additive white Gaussian noise is considered. The key parameters of the VLC system are given in Table III. Subsequently, the receiver movement within the illuminated region is evaluated using a predesigned equivalent-receiving plane (explained in the next section), hence, the motion path of the user is depicted in Fig. 22. The tracking video was then processed in MATLAB where the optical tracing including the subtraction algorithm, and the blob analysis is applied to extract the positions of receiver in the image plane (or screen) where the area of the receiver is set initially in Pixel units highlighted in Table IV, and hence being equivalently mapped into the room-scale. The optical tracking system parameters are outlined in Table IV.

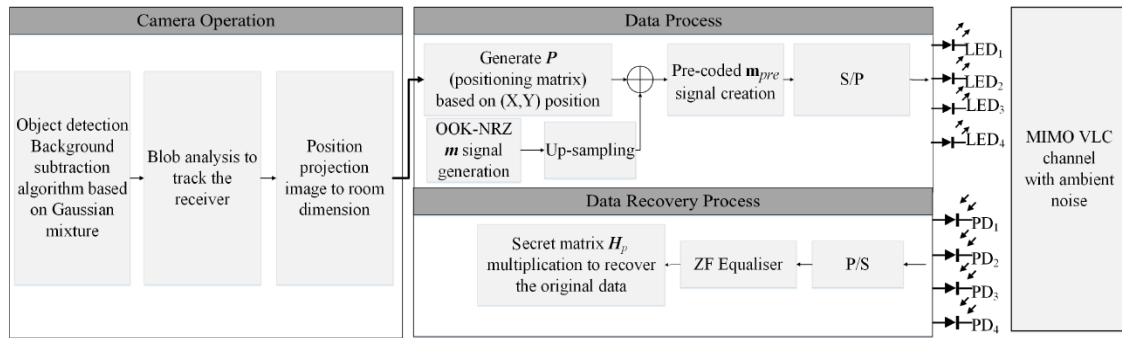


Fig. 21. Block diagram of the proposed system.

Room dimension	
Length(m)×width(m)×height(m)	5×3×3
Parameters	Values
Number of LED-based transmitters	4
Transmitters locations	(1.25, 1.25),(1.25, 3.75) (3.75, 1.25),(3.75, 3.75)
LED Type	SR-01-WC310
Beam angle-based transmitter	120°
Number of sample (n)	10
LED Bandwidth	3 MHz
Data rate (R <sub>B</sub> )	5 Mbit/sec
Transmitter gain	20 dB
Number of LED-based receivers	4
Receiver moving speed	0.53 m/s
Receiver dimension	10 cm × 10 cm
PD active area	15 mm <sup>2</sup>
PD responsivity	0.6
PD field of view (FOV)	180°
Receiver sensitivity (used with AD8015 transimpedance amplifier)	-30 dBm
LPF cut-off frequency	0.7 * R <sub>B</sub>
X-Y sweep resolution	1 cm × 1 cm
Noise parameters	
Equivalent noise bandwidth	R <sub>B</sub> Hz
Background Current	500 × 10 <sup>-6</sup> A
Noise bandwidth factors(I <sub>2</sub> , I <sub>3</sub> )	0 : 562; 0 : 0868
Absolute temperature	313 kelvins degree
FET channel noise factor	1.5
FET transconductance	30 × 10 <sup>-3</sup> mS

TABLE III. VLC SYSTEM PARAMETERS.

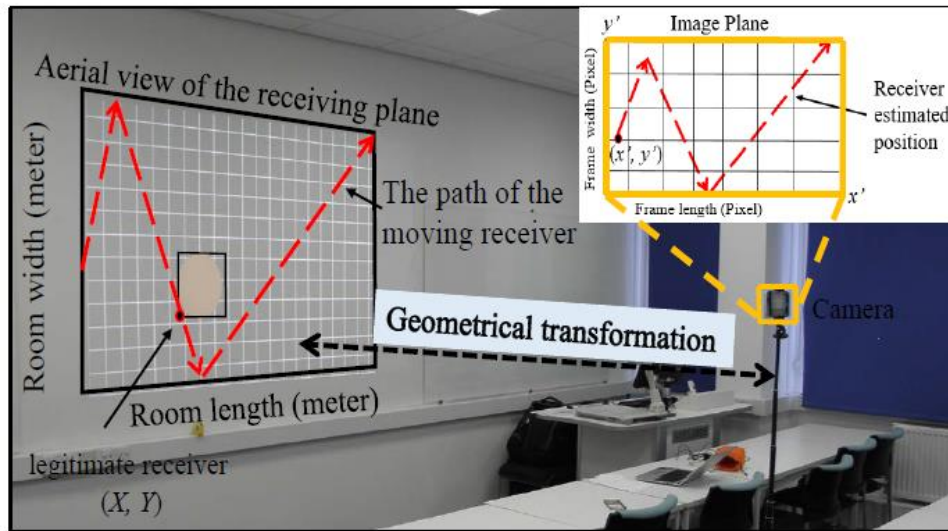


Fig. 22. Experiment set-up.

Parameters	Values
Camera sensor	12 MP CMOS
Focal length	4.2 mm (26 mm eff)
Pixel size	1.4 $\mu\text{m}$
Max aperture	F/1.7
Resolution	320 $\times$ 240, 640 $\times$ 480, 720 $\times$ 576, 1280 $\times$ 720
Frame rates	25 Fps
Measured ambient level(lux) (Note: ISO office standard)	2 LUX (No light), 275 LUX (Low light), 450 LUX (Indoor normal light)
Camera height (h)(i.e. distance between camera and receiver plane)	2 m, 3 m
Camera location	(2.5,2.5)
Camera field of view (FOV)	90°, 67.3°
Number of Gaussian modes (used in the MOG model)	3
Number of initialisation frames (used in MOG model)	50 frames
Minimum blob area for 320 $\times$ 240	500 pixels
Minimum blob area for other resolutions	2000 pixels

TABLE IV. OPTICAL TRACKING SYSTEM PARAMETERS

### Implementation Strategy

The process of camera position self-determination to locate the authenticated receiver, within its receiving field of view, and the encryption process is presented in Fig. 22. Likewise, a projection has been used to display (or mimic) a moving user on the screen, which is equivalent to a user moving on a room's floor. The camera is to monitor an equivalent-receiving plane (in MIMO VLC system) with different link distances, camera resolutions, and various illumination levels of the environment as given in Table IV. For the sake of simplicity and to avoid the usage of the perspective transformation, the camera is positioned in the projected center of the screen (i.e. room floor equivalently) from a distance  $h$  to form a collinear photogrammetric measurement (an object point and its photo image all lie along a straight line) between the receiver plane and the camera frame as depicted in Fig.

22. The mapping from the screen/camera setup to the MIMO VLC system is shown in Fig. 22. The conversion scale is obtained through the utilization of mathematical equations [Publication J1]. Correspondingly, the image plane displays an aerial view of the designed scene and the illuminated region in the room, where the receiver positions and moving route are detected to facilitate the evaluation between the actual and estimated location of the legitimate receiver. The room is normally lit by other artificial fluorescent lamps at 400 Lux level. The receiver is then able to recover the transmitted signal at the designed communication zone, whereas, at other positions outside this zone, data recovery is not feasible. The system performance is investigated by performing different tests using various camera resolutions, transmission link including the camera, and multiple-level light conditions for each position of the receiver. BER vs SNR curve for the legitimate and eavesdropper receiver positions in the illuminated region were obtained.

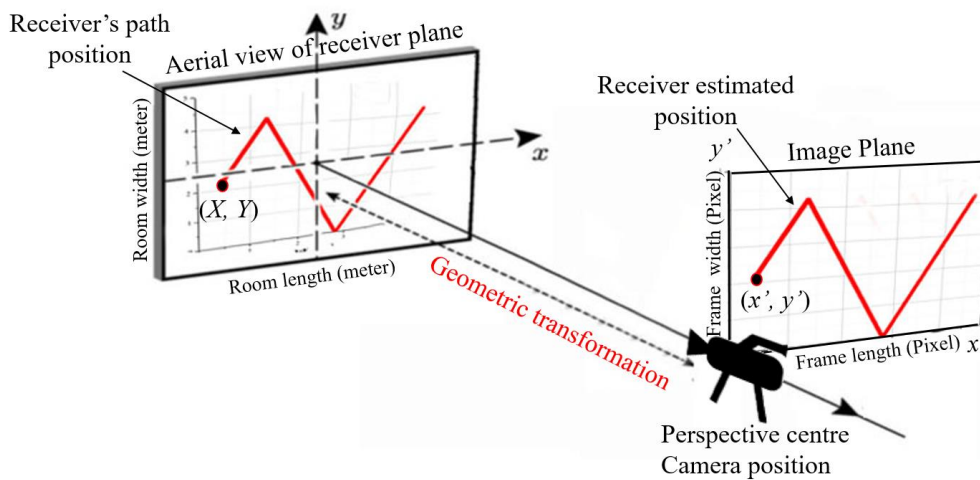


Fig. 22. Geometrical transformation between the image plane and the room dimensions.

Resolutions	Error Mean X(cm),Y(cm)	Standard Deviation X(cm),Y(cm)	Maximum Error X(cm),Y(cm)
1280 × 720	2.44, 2.28	1.86, 2.07	15.23, 7.92
720 × 576	2.44, 2.25	1.81, 2.06	14.63, 7.81
640 × 480	2.52, 2.24	2.16, 2.06	19.53, 7.92
320 × 240	2.53, 2.14	2.73, 1.87	37.89, 7.92

TABLE V. TRACKING SYSTEM PERFORMANCE WITH DIFFERENT RESOLUTIONS

### Results and Discussions

Firstly, we experimentally evaluate the position tracking performance, which is one of the key elements in the proposed dynamically secured MIMO VLC system. Figure 23 shows the experimental performance evaluation of the tracked moving receiver with different camera resolutions at various positions in the moving path. The practical results indicate that the average positioning error occurring between the original and the recorded scene for the lowest camera resolution (320 x 240) in a Cartesian coordinates system is (2.53cm, 2.14cm). Correspondingly, the measured standard deviation and maximum error values correspond to this under test resolution are (2.73, 1.87), (37.89, 7.92) respectively. For other higher camera resolutions, the corresponding system performance is summarized in Table VI. Also, the

minimum error value between the original and the recorded values with different resolutions is (0 cm). Note that though the resolutions are different, the errors seem to be converged and largely unvaried, the usage of the blob shape in the localization of the moving receiver minimizes the positioning errors. This investigation indicates that we could use a low camera resolution for the proposed system, hence reducing the complexity, cost, and computational power requirement.

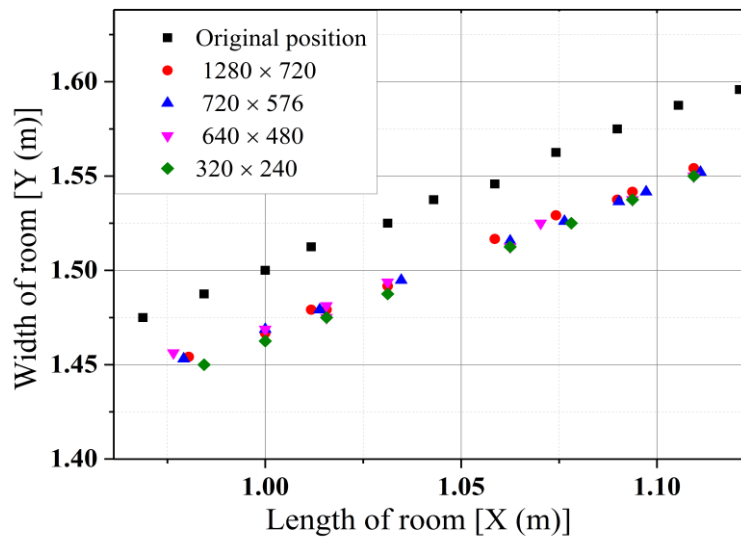


Fig. 23. Zoom in evaluation of the receiver tracking position for different camera resolutions (distance =2m, lux=0).

A further test is carried out to determine the effect of the outdoor ambient light intensity level (i.e., ambient noise) on the camera tracking system since the user might move/walk to different areas where the illumination levels are not the same. In this type of test, we experimentally measure the system performance in different ambient noise levels. The lux meter was placed at the receiver location (i.e., receiver plane) in order to estimate the real value of the ambient noise prior to initializing the tracking operation. Different lighting levels will lead to a fluctuation of the camera's position detection performance. Low light circumstances will create a large noise in the acquired image, and that affects the accuracy of our proposed localization scheme. Results illustrated in Fig. 24 as well as in Table VI present the error of the positioning determined in the proposed tracking system with the ambient noise level of (450, 275, and 0 lux, i.e. standard lighting, dimming and dark conditions). The lowest accuracy of the positioning system occurs when lux = 0 (i.e. no light at the receiver, where the background subtraction method in the camera does not perform well). In a dark condition, the observed x-axis maximum error is (12:5cm) compared with (6:64cm) error with normal indoor light conditions. Hence in a well-lit room, the tracking is much more reliable with regard to the camera's resolution.

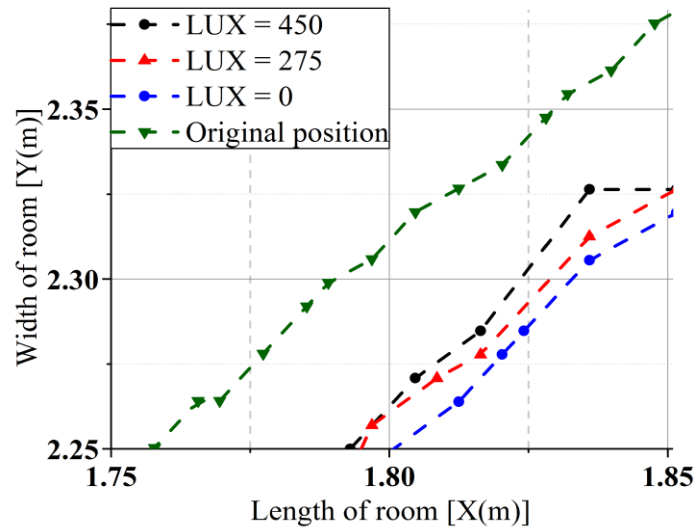


Fig. 24. The zoom-in effect of various ambient noise illumination levels at the receiver on the camera-based tracking performance with (distance =2m, and resolution =1280 x 720).

Illumination (Lux)	Error Mean	Standard Deviation	Maximum Error
	X(cm),Y(cm)	X(cm),Y(cm)	X(cm),Y(cm)
450	2.54, 1.37	1.26, 1.27	6.64, 6.66
275	3.72, 1.03	1.41, 0.99	6.64, 5.41
0	2.47, 1.46	1.33, 1.19	12.5, 5.41

TABLE VI. TRACKING SYSTEM PERFORMANCE OF VARIOUS LIGHT INTENSITIES

Figure 25 (left) presents a motion path of the authenticated receiver (user) inside the illuminated region. The motion path includes 160 tracked points. The transmitter sends a signal with a length of 1000 bits at each of the tracked points. The number of samples per bit is 10. The security performance of the system is measured by means of BER calculation at the receiver side, the BER obtained in Fig. 25 (right) for the user when moving along the path is minimized ( $BER < 10^{-5}$ ) as the transmitter adaptively designs the secured communication channel to follow the motion path of the legitimate user. The beam-width of the secured communication zone is approximately 6 cm with respect to x and y coordinates which shows a very good physical security performance of the link. The transmitted and estimated signals by an individual PD at the legitimate user is showed in Fig. 26(a), whereas the recovered signal by an individual PD at the eavesdropper is depicted in Fig. 26(b). The successful demonstration has shown that the proposed dynamically secured MIMO VLC system operates properly when incorporating the position tracking approach under user movement scenarios. Finally, we experimentally reconfigure the distance between the camera (in the transmitter side) and the user (in the receiver plane). The measurement results show that an average position error is (3:5cm, 5:21cm) for the distance h of 2m and 3m respectively as shown in Fig. 27.

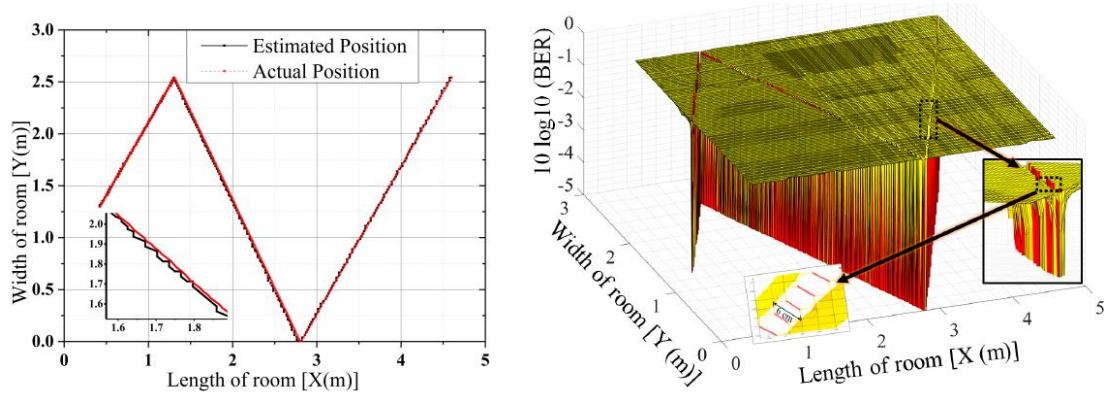


Figure 25. (left) comparison between the actual and the estimated position for the entire room. (right) BER mapping for (resolution = 1280 x 720, distance = 2 m, and normal indoor light condition Lux= 450).

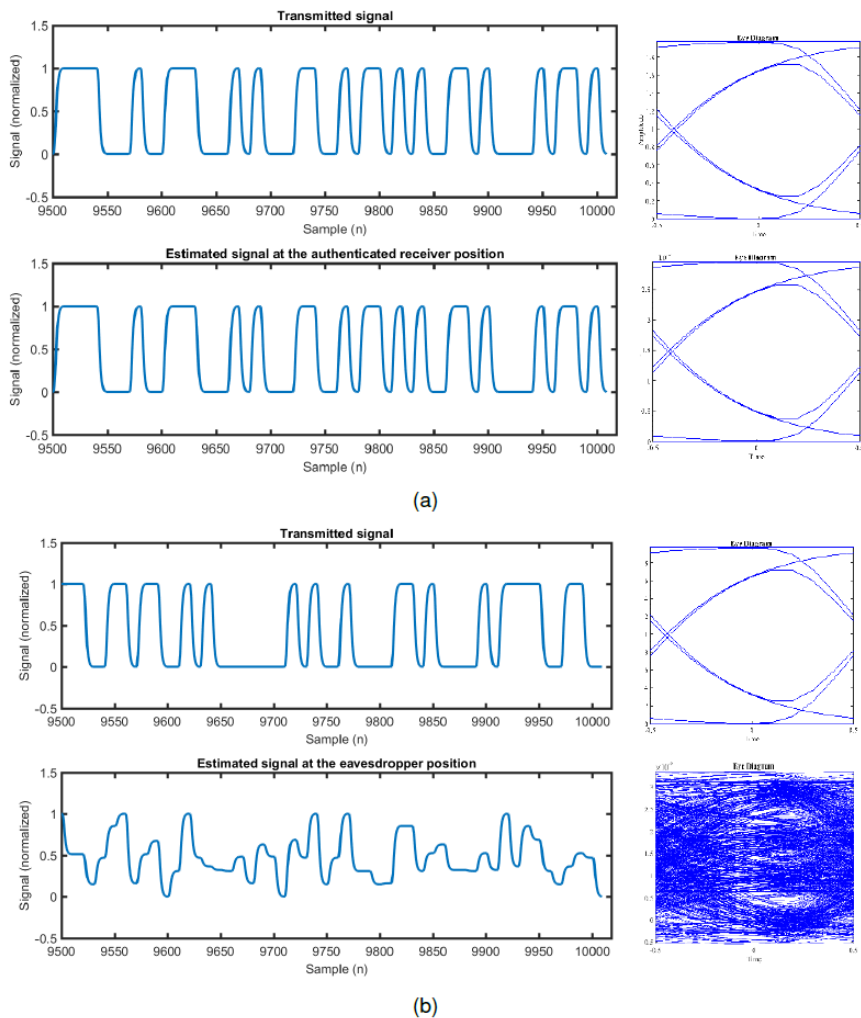


Figure 26. The transmitted and estimated signals and the eye diagram of an individual PD receiver for (a) The legitimate user. (b) The Eavesdropper.

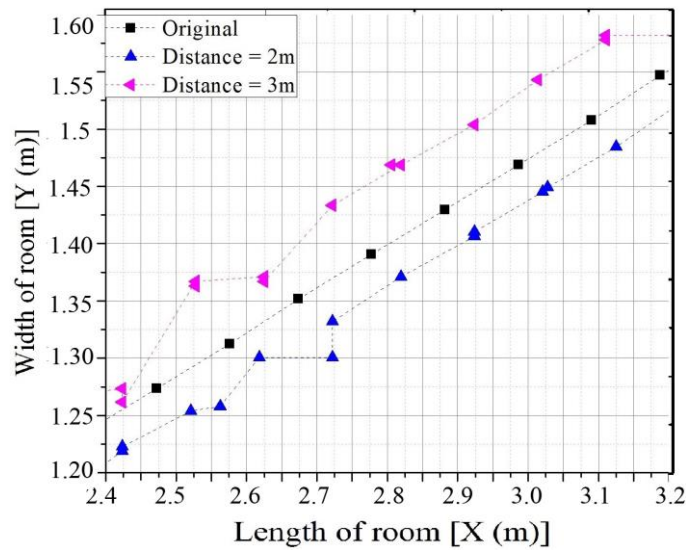


Fig. 27. The effect of different distance between the Camera-based surveillance system and the receiver plane for (resolution = 1280 x 720, distance = 2m, and normal indoor light condition Lux = 450).

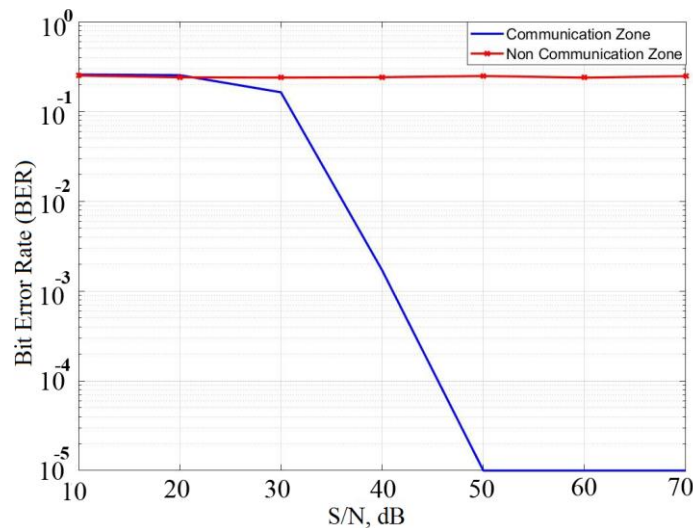


Figure. 28. BER against SNR for the MIMO VLC system for different position of receiver (inside and outside the communication zone) with (resolution = 1280 x 720, distance = 2m, and normal indoor light condition Lux = 450).

The proposed algorithm can work properly with respect to these ranges, hence, low BER accuracy (at  $10^{-5}$ ) can be maintained within these ranges as depicted in Fig. 25(right). Note that, BER is estimated for different SNR conditions since Fig. 28 shows that the receiver in the communication zone is able to recover the transmitted data with SNR more than (40 dB) for the resolution of 1280 x 720, distance of 2m, and normal indoor light condition of 450 Lux, whilst the eavesdropper in the non-communication zone is incapable of recovering the data. The speed of detection varies according to the number of recorded frames, minimum blob area that been set, and the light condition in the room, however, the P matrix average estimated generation time based on MATLAB was 188  $\mu$ s, whereas the standard deviation was 120  $\mu$ s using Intel Core i5-6200 with 4GB RAM (LENOVO - 80TY ), therefore, the system

can accommodate a real-time moving receiver. The system can be implemented using the integrated circuit design (i.e., field-programmable gate array (FPGA)) platform which could outperform the graphics processing unit (GPU) utilized in this study.

## **C. Visible Light Communication based Indoor Localization**

### **Introduction**

In recent years, the indoor positioning system (IPS) has received much interest in smart home applications. The benefit of this system is to specify the location of the things or navigation, which is a very useful system either in a shopping center or an industrial factory. There are many types of indoor positioning system such as Bluetooth, RFID, Wi-Fi, Visible light communication. The application of visible light communication in IPS has the advantage of improved accuracy, since there is no electromagnetic interference. The transmitters can be used as a general lighting system along with high speed data communication, in addition to transmitting positional data. Multiplexing methods for positional data such as FDM and TDM, have been proposed, but these two methods have limitations in terms of scalability and the difficulty of synchronization. Therefore, code division multiplexing allows greater scalability and each LED may be asynchronously modulated. The receiver in VLC indoor positioning systems using may either be a photodetector or a CMOS camera in a smart device. Positioning algorithms in photodiode based IPS, relying on either received signal strength (RSS), time of arrival (TOA), and angle of arrival (AOA) data, vary in complexity and accuracy. The accuracy is excellent; however, the system depends on power of light, complexity in estimating the position and creating dedicated receiver circuits. On the other hand, the camera based IPS is attractive because the receiver does not need additional equipment, where the CMOS camera sensor on any common smart handheld device may be used. Rolling shutter effect can be used to detect high frequency data modulation of the LEDs that cannot be perceived by the naked eyes. Thus, this phenomenon has also been used in the positioning system application. In this work, we developed a three-dimensional VLC indoor positioning system using smart device camera receiver whereby the rolling shutter effect of CMOS camera sensor to detect the encoded identification data and necessary information regarding transmitter positions from the individual LEDs. No prior assumptions have been made regarding each LED transmit power, this allows for non-identical LEDs and their power deterioration over time. Images of 4 LEDs are required to estimate the receiver position in 3 dimensions. In the image capturing process, it is necessary to adjust the exposure setting. The captured images are processed by converting them to black and white where the black and white stripes may be decoded. Then by applying a different threshold, we propose a method to use the white pixel area (counted in number of pixels), corresponding to each LED image, to estimate the distance between each LED and the receiver. These estimations are used in trilateration algorithm to determine the receiver position. Through proper calibration, the position error is within 10 cm.

### **System implementation**

We carried out experiment in a setup shown in Figure 29, for the scaled down demonstration of the system. Four LEDs, as position beacons, are located in  $50 \times 50$  cm<sup>2</sup> square, the LEDs' plane is 1.3 m above the table. Each LED is modulated by a different 16-bit Manchester code as identification data. The diagram of modulator and driver is shown in the Figure. The maximum modulating data rate is 187 kb/s, using receiving camera at 60 fps. In practice, the

LED is modulated at a lower rate since, at a larger distance the reduced intensity can limit the detection. The testing point grid is also shown in Figure 30. During the experiment, other ambient light was reduced. The camera was placed at various heights to test the position accuracy in 3-dimensions. The origin (0,0,0) is defined as the center of the table at 130 cm below the LEDs' plane.

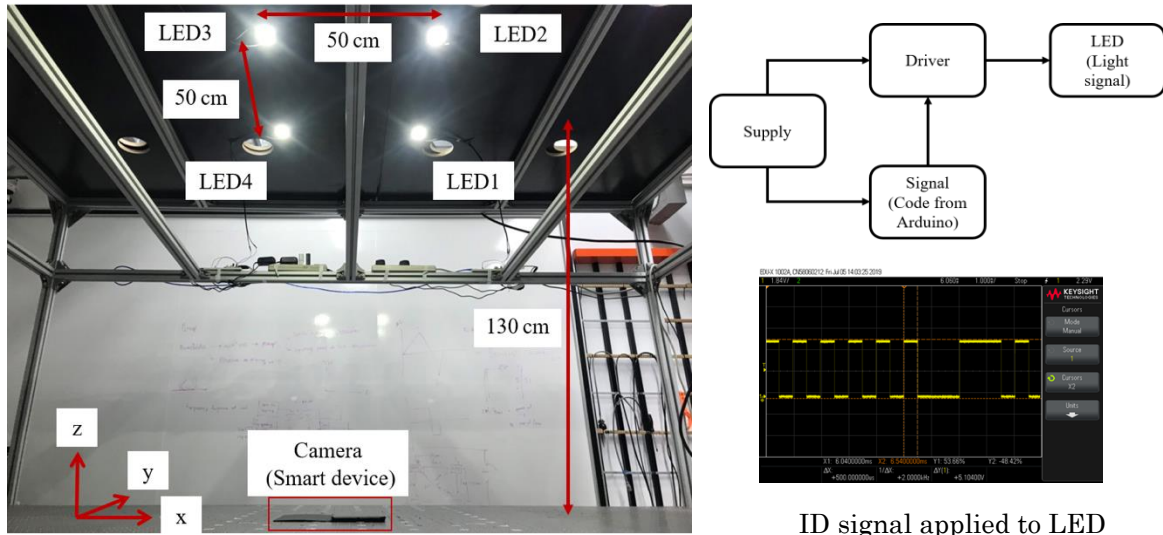


Figure 29. LEDs' plane and tablet camera on the table.

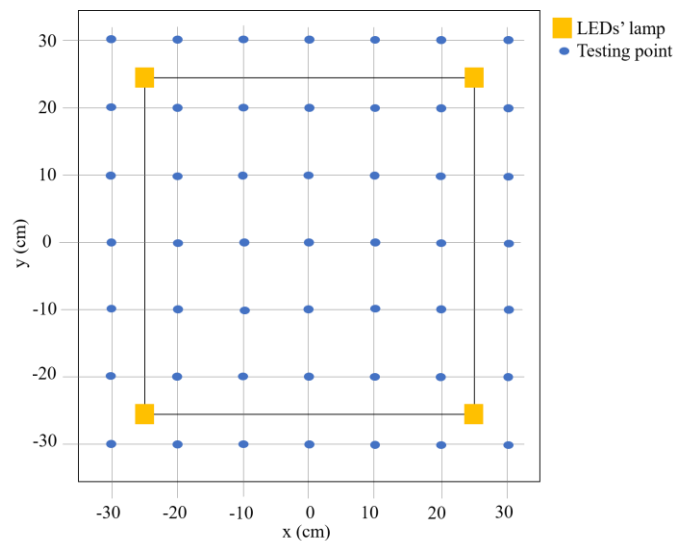


Figure 30. Testing point coordinates.

In the captured image of Figure 31(a), each LED shows different black and white stripes according to the modulating code, which can be used to identify the LED beacons. Then distances to the LEDs are estimated by shape and size of the white pixels, as shown in the graph of Figure 31(b). The position of the receiver is estimated by a simple trilateration algorithm as in Figure 31(c). Details of the algorithm is presented in Publication [x](#). Calculations are coded in the Android tablet device. The application outputs the estimated distances to the LEDs and the calculated receiver 3D position shown in Figure 31(d).

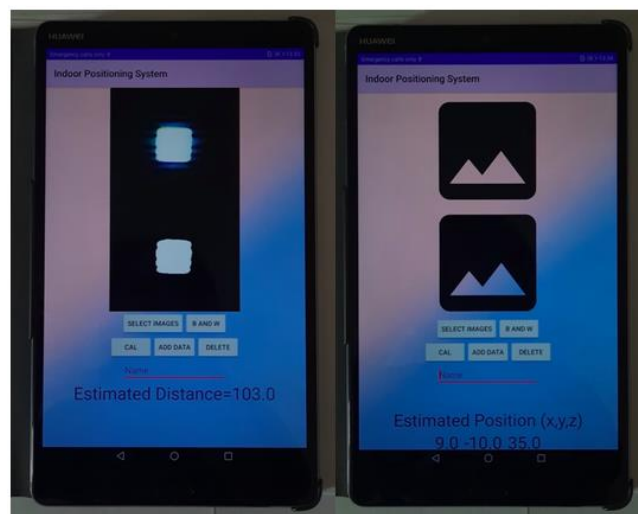
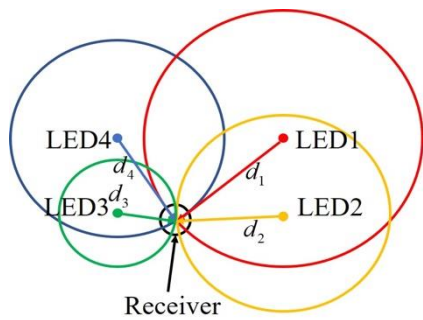
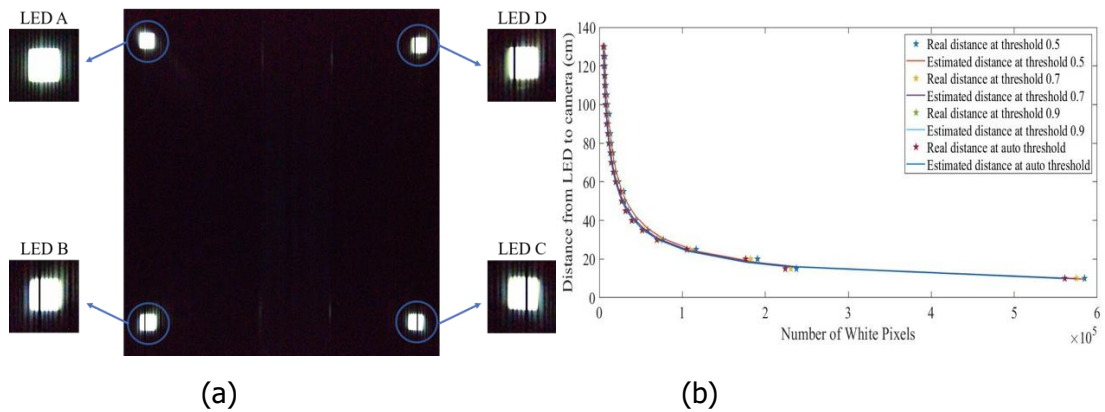


Figure 31. Position estimation algorithm and smart device application

### Position error measurement

The estimated position error in 2D and 3D at various grid locations are shown in Figure 32 and 33 for the distance of receivers from floor of 20 cm and 30 cm respectively. There were maximum errors in 3D and 2D position of 64.39 cm and 62.09 cm, respectively. It is due to shorter distance  $d_i$  that was estimated using white pixel calibration method. With the introduction of error term, which is a function of number of white pixels, since it is found that the distance is systematically underestimated, we could estimate the positions of the receiver on the grid more precisely as in Figure 34 and 35. The accuracy of the estimated position of receiver has been improved greatly. 73.47% of estimated positions in the grid are within 5 cm error and 100% of estimated positions in the grid are within 10 cm error. In 2 dimensions, the average position error is 4.35 cm and 3.28 cm at  $z = 20$  cm and 30 cm respectively. In 3 dimensions, the average position error is 4.53 cm and 3.50 cm at  $z = 20$  cm and 30 cm respectively.

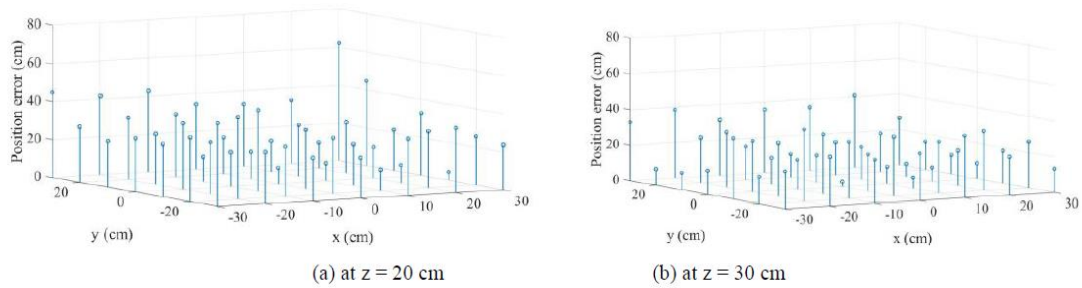


Figure 32. Position error in 2D of camera.

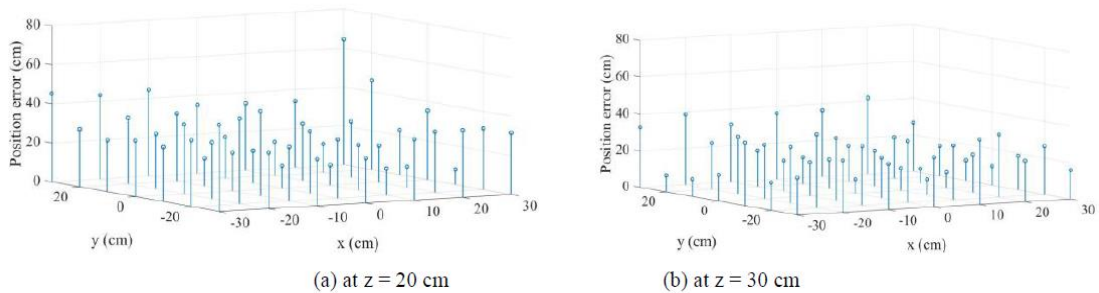


Figure 33. Position error in 3D of camera.

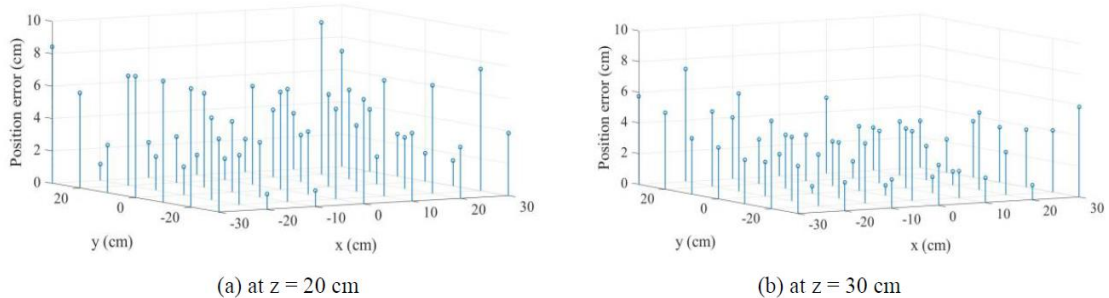


Figure 34. Position error in 2D of camera after compensation

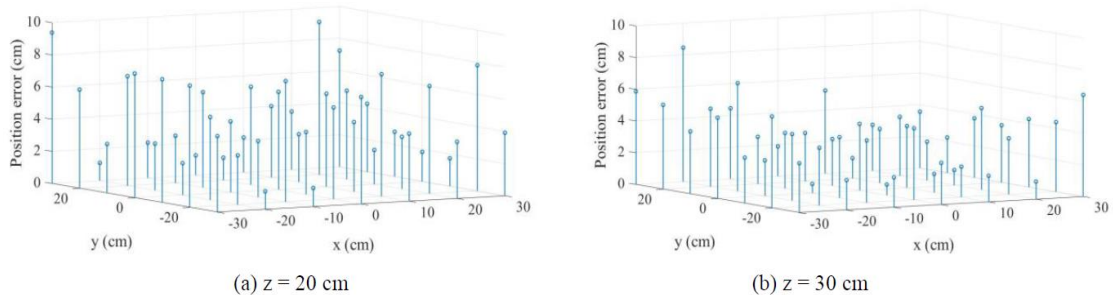


Figure 35. Position error in 3D of camera after compensation

## Conclusion

We developed and demonstrated a three-dimensional VLC indoor positioning system using a smart device camera receiver and positioning method with image processing. We considered the suitability of the camera settings and the threshold for LED identification and calibrating the distance between the LED and the camera for using in the position estimation algorithm.

This proposed system can estimate the position with low complexity. If the test volume is scaled up to the actual room size the absolute error should be larger. However, it should still be possible to determine reasonably accurate position relative to the LED beacons within the room. The system may be applied to indoor localization and navigation. For example, room and hallway lighting LEDs may be modulated with positioning signals, so that a smart device may be used to receive the signals from its camera to navigate the user inside a building, where the GPS signals are unreachable and too erroneous.

## D. Visible Light Communication Networking

### D.1. PHY/MAC Cross-Layer Analysis for IEEE 802.15.7 Uplink Visible Local Area Network

Supported by IEEE 802.15.7 standardization activities, visible local area network (VLAN) has been gaining popularity in recent years. Specified in the standard are physical (PHY) and uplink medium access control (MAC) layers of VLAN. However, there is a lack of studies on the MAC performance analysis and improvement under the effects of PHY transmission errors in the literature. Motivated by the above discussion, the main goal of this work is to introduce a unified framework of PHY/MAC cross-layer analysis, shown in Fig. 36. To the best of our knowledge, this is the first study for the IEEE 802.15.7 standard, in which its uplink MAC performance analysis and improvement under the effects of PHY transmission errors are discussed. More specifically, the contributions can be summarized as follows:

- Consider the critical differences between IEEE 802.15.7 and previous standards, we derived a new cross-layer analysis. From the PHY-layer perspective, the analysis incorporates the effects of VLC channel, that differs from RF channels of both IEEE 802.11 and IEEE 802.15.4. From the MAC-layer perspective, our analysis takes into account modifications in (i) the backoff algorithm that differs from the one of IEEE 802.11, and (ii) the carrier sensing mechanism that differs from the one of IEEE 802.15.4.

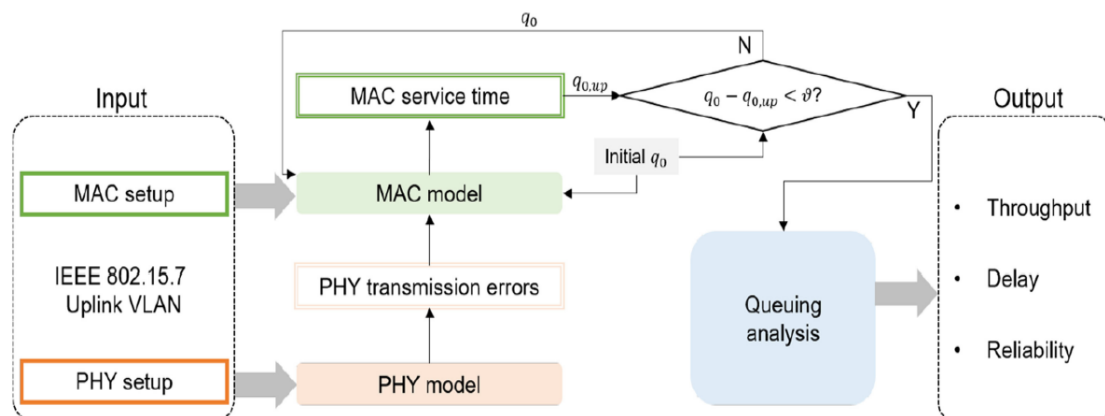


Figure 36. Methodology of IEEE 802.15.7 PHY/MAC cross-layer analysis.

- To improve the performance, we considered the use of frame retransmissions. It is worth mentioning that though MAC enabling frame retransmissions is already specified in the IEEE 802.15.7 standard, it was often omitted in previous studies due to the assumption of no PHY transmission errors. To do so, we proposed a three-dimensional (3-D) Markov chain model for analyzing the MAC performance, which extends previous analytical models of

IEEE 802.15.7 MAC, e.g., 1-D Markov chain and 2-D Markov chain, by (i) adding a dimension for retransmission states and (ii) taking into account PHY transmission errors in state transitions.

- The proposed model allows the derivation of various system performance metrics, including delay, reliability, and throughput. Based on these metrics, we discuss a cross-layer optimization, where the maximum number of retransmissions is selected by a trade-off between the PHY loss reduction and the MAC service time increment. As confirmed in the numerical results, MAC performance is critically affected by PHY transmission errors, and frame retransmissions, with a proper selection of the maximum number of retransmissions, could considerably improve the performance.

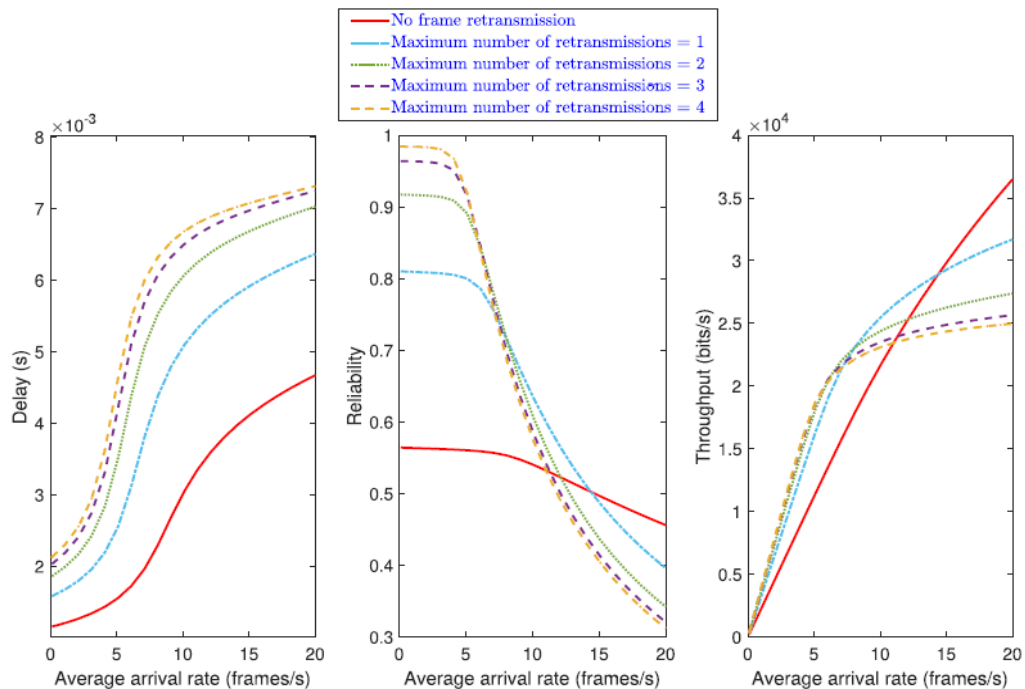


Fig. 37. Effects of frame retransmissions on MAC performance (number of users is 4).

We thoroughly analyze the MAC for various performance metrics taking into account PHY transmission errors due to different VLC physical factors. We also considered MAC enabling frame retransmissions as a solution to PHY transmission errors. Numerical results show that, first, MAC performance is critically affected by PHY transmission errors and, second, frame retransmissions, with a proper setup, could considerably improve the performance, as shown in Fig. 37.

### **D.2. Analog network coding aided multiuser visible light communication networks using optical CDMA**

Previous studies mainly focus on analyzing the performance of optical code-division multiple-access (OCDMA)-based VLC systems using different type of optical codes. Accordingly, the performance analysis only takes into account the impact of multiuser interference, which is governed by code's properties. However, in order to evaluate the feasibility of multiuser VLC networks using OCDMA, it is necessary to investigate a more

practical scenario, where the VLC channel model, the VLC transceiver’s parameters, and the bidirectional transmission protocol are considered. Motivated by this lack of investigation, the main goal of this study is to propose a novel architecture for an indoor VLC network that can support bidirectional transmission for multiple users in a room. More specifically, the contributions of this paper can be summarized as follows:

- We propose a VLC network architecture that supports the data exchange among the users inside a room as shown in Fig. 38. In this scenario, there is the case that there is no line-of-sight (LOS) connection among the users due to obstructions. As the solution to this problem, we propose to use a coordinator mounted in the ceiling, which plays a role as the relay node receiving the signal from one user and then forwarding it to other users. To connect this network to the Internet, one gateway node is connected to the coordinator for decoding the signals from multiple users and then forwarding them to the Internet and vice versa.

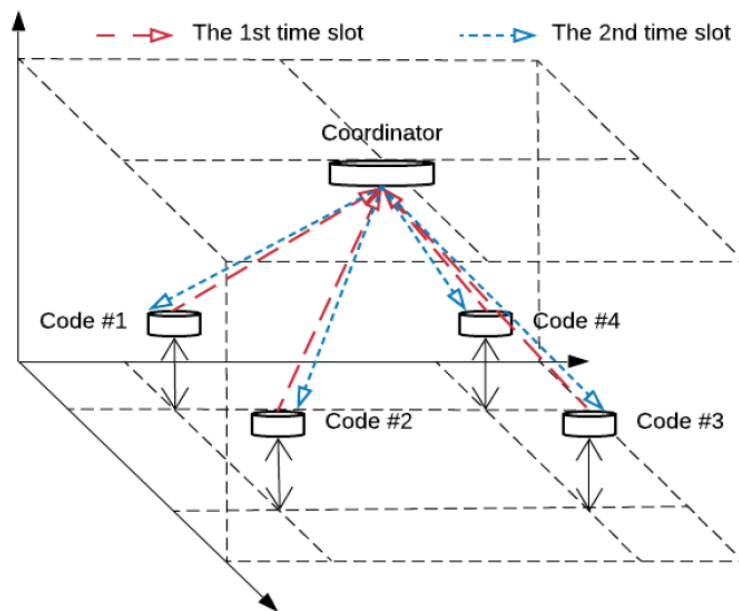


Figure 38. The proposed VLC network using ANC and OCDMA.

- We design a protocol that provides bidirectional half-duplex transmission based on analog network coding (ANC) and supports multiple users with the help of OCDMA. The conventional scheme of bidirectional half-duplex transmission needs four time slots to exchange packets between two users while ANC only requires two time slots. Thanks to the reduction of needed time slots, our proposed VLC networks can achieve larger throughput.
- We derive the mathematical expression for BER and throughput of the proposed VLC network taking into account the indoor VLC channel model, the VLC transceiver’s parameters, the impact of noise and interference. The obtained mathematical expressions can be used to investigate the network performance versus various physical layer parameters to evaluate the feasibility of the proposed VLC network.

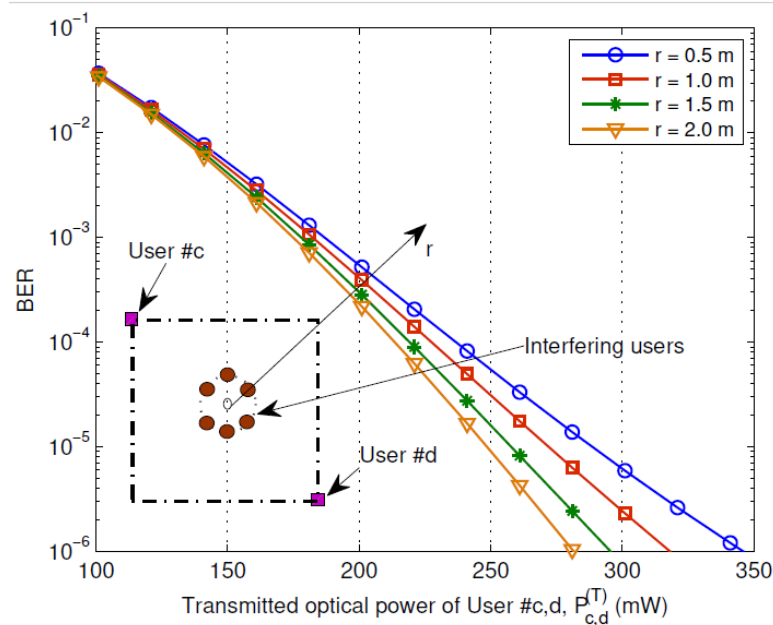


Figure 39. BER versus the transmitted optical power of desired user #c, d with 6 interfering users, whose distance from the room center is r.

The numerical results, as shown in Fig. 39, demonstrated that low BER and high network throughput can be achieved in our proposed network. Based on the numerical result, we can determine the required transmitted optical power, the number of supportable users, and the suitable value of VLC transceiver's parameters such as the half power semi-angle and FOV, which are useful information for designing indoor multiuser VLC networks.

### E. Ultra-high-speed indoor communications

In 6G and beyond networks, which can be deployed in 2030 and later, to facilitate unprecedented demands for new services such as "ultra-high-fidelity" virtual reality or holographic communications, which will demand data rates in the order of Terabits/s, an ultra-fast optical wireless access system in the infrared spectrum is very important. The system should be able to offer capacities up to several hundred Gigabit/s to Terabit/s with a wide field-of-view to provide sufficient network coverage. This can be realized by developing a narrow-beam fiber-wireless-fiber system using beam steering and automated alignment capability for localization and tracking of user terminals. In order to achieve ultra-high capacity up to Terabit/s, the use of advanced modulation formats and wavelength division multiplexing are also very promising. A hybrid and quasi-parallel transmission with ultra-high-speed radio communications will also be attractive to improve the communication reliability and coverage. In addition, a cascaded optical wireless and radio communication in high frequency bands, in which OWC links are used for high-speed and flexible backhaul transmission and radio links are used as broadband access to user terminals, will be another important solution. In this subsection, we present our research works on ultra-high-speed indoor communications using optical wireless communications (OWC) in the infrared spectrum, and a hybrid OWC and millimeter-wave system for high reliability communications.

### E.1. Ultra-high-speed indoor optical wireless system

#### Experimental setup

The experimental setup for high-speed signal transmission over an OWC system is shown in Fig. 40. In the experiment, we transmitted signals over the OWC system using two different wavelengths to increase the capacity. In addition, advanced modulation format using a Nyquist-subcarrier modulation signal was employed. The signal consists of 10 subcarriers with a total bandwidth of 10 GHz centered at 7.5 GHz, was generated in MATLAB and downloaded to an arbitrary waveform generator. The signal is amplified using a driver amplifier before modulating the combined optical signal from two different laser diodes. To minimize the fiber dispersion effect, an optical IQ modulator is used to generate an optical single-sideband with carrier-suppression signal. The modulated optical signal is amplified using an optical amplifier and transmitted over a single-mode fiber cable to a remote antenna. The signal is thereafter emitted directly in free space using an OWC antenna. After being transmitted over approximately 5 meters in free space, the signal is received by another OWC antenna and focused directly to a fiber. We should note that, for this proof-of-concept demonstration, the signal was focused to a fiber cable at the receiver. However, in practical systems, a photodetector or an array of photodetector should be used. The received signal is then amplified by another optical amplifier, filtered, and detected by a photodetector. The detected signals are input to a real-time oscilloscope and are analyzed offline.

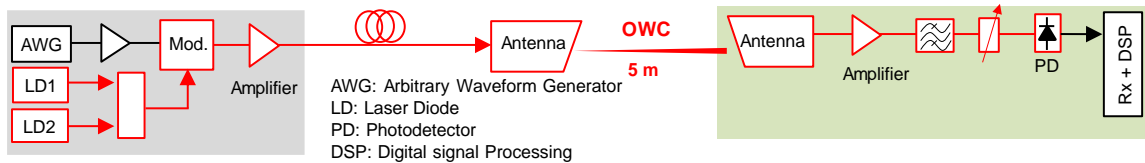


Figure. 40. Experimental setup for high-speed indoor optical wireless communications.

#### Experimental results

Figure 41 (a) shows an example of the received optical power measured at the output of the receiver OWC antenna. A stable received optical signal with a power variation of less than 1 dB could be observed. Figure 41(b) shows the performance of the OWC system for different additional losses. In the experiment, the additional loss was adjusted using a variable attenuator inserted at the output of the receiver OWC antenna. The additional loss can emulate attenuation in the OWC link owing to vibration or misalignment. The error vector magnitude (EVM) shown in the figures is the averaged value of those from all subcarriers. Two 32-Quadrature amplitude modulation Nyquist-subcarrier modulation signals with a total capacity of 100-Gb/s are successfully transmitted over the system. It should be noted that, in the experiment, we did not apply any signal-signal beat interference suppression method, which is considered relatively high in an optical single-sideband system using direct detection. Only a simple pre-emphasis was applied to compensate for the non-flat frequency response. Figure 41(c) shows example of the received spectrum of the signal after being transmitted over one of the two OWC channels with and without applying pre-emphasis at the transmitter. We expect that the system performance, the transmission capacity, can be significantly improved when an appropriate method is applied to mitigate the signal-signal beat interference. We also observe that when the loss in the OWC system increases, the system performance is considerably degraded because of the reduction in the signal-to-noise ratio.

This indicates that the operation availability of the transmission using OWC systems can be reduced under severe attenuation conditions.

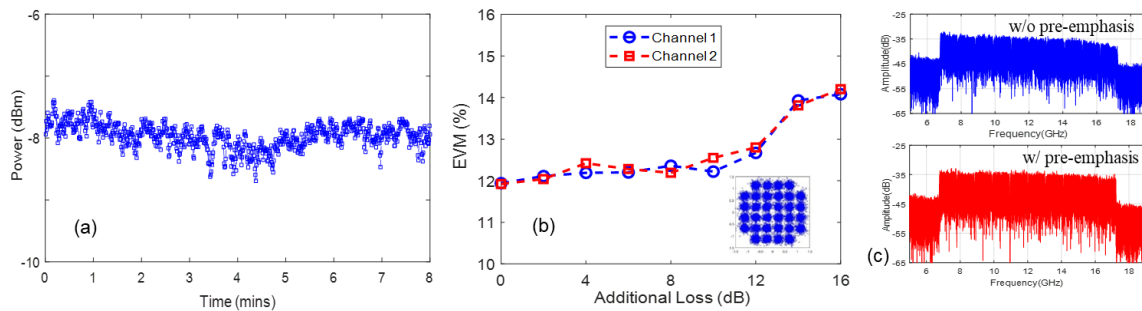


Figure. 41. Experimental results: (a) received power of the OWC system; (b) OWC system performance, (c) received signal spectrums.

## E.2. Cascaded optical wireless and millimeter-wave communication

### Introduction

High-efficiency and ultra-high-speed indoor communication is an essential element in future wireless networks, such as beyond 5G and 6G. Several solutions have been proposed to develop such a high-speed network, including radio access network (RAN) using high carrier frequency in the millimeter-wave (mmWave) bands; light-fidelity (Li-Fi) network using visible light communications; high-speed optical wireless communication (OWC) using narrow laser beams; and hybrid Li-Fi and radio network. The solutions can provide a relatively high data rate network; however, several disadvantages and challenges must be overcome. For the RAN in high-frequency bands, owing to high atmospheric attenuation, requirements on link budget, transmit power, and complexity of the indoor backhaul network must be considered. For the Li-Fi and hybrid Li-Fi/radio networks, it is difficult to provide a capacity of greater than 10 Gb/s to users due to bandwidth limitation. For the narrow laser beam system, focusing and coupling the incoming optical beams to users' terminals from free space face many challenges. A very accurate position information and a highly complicated tracking system are indispensable. To provide an ultra-high-speed communication to indoor users, thus, a new transmission method should be developed, which should be capable of providing an ultra-high-speed, low-latency, and energy-efficient communication using a simple control and management system.

In this work, we proposed a new transmission method using a novel hybrid, cross spectrum, and cross medium of optical fiber, mmWave, and OWC systems. In the system, a RAN using ultra-small radio cells in the mmWave band is proposed for communications with end users, and a flexible and ultrafast fiber-OWC system is employed for the transmission of the mmWave radio signals from a cloud to antenna sites. As a proof-of-concept demonstration, we successfully transmitted approximately 40 Gb/s mmWave signal in the 100-GHz band over a seamless fiber-OWC system, consisting of 20-km single-mode fiber (SMF) and 1-m OWC link. The proposed system can provide an ultra-fast, energy-efficient, and low-latency communication solution for future ultra-high-speed indoor networks.

### Concept of the cascaded OWC-millimeter-wave system

The concept of the proposed system is shown in Fig. 42. In the system, a dual-hop access

network using OWC and radio links in the mmWave band is proposed. The radio links work as the access network for communication with users, while the OWC links are used as the extension of fiber links for the flexible and easy transmission of radio signals from a home network center (HNC) to access points (APs). In addition, to reduce latency and simplify APs, a seamless fiber–OWC–radio system is proposed using a radio-over-fiber technology. In this method, an optical mmWave signal is generated at the HNC and transmitted over fiber links to relay nodes (RNs). At the RNs, the signal is emitted directly into free space using OWC terminals. The OWC signals are thereafter transmitted from RNs to APs which are installed close to end users. At the APs, the OWC signals can be received and seamlessly converted to radio signals in the mmWave band using a high-speed photodetector (PD) or a PD array. The mmWave signals can be amplified and transmitted directly to the end users without having to perform any signal conversions and processing. This makes the system simple, resulting in low transmission delay and power consumption. Using the proposed system all the signal generation and processing functions can be conducted at the HNC. The RNs and APs can be very simple. Furthermore, the APs are located at fixed locations, thus, the OWC beam steering and controlling can be performed much easier than to the user terminals as in the previous systems. The APs can also utilize advanced receivers, such as large-coupling-area PDs and PD arrays, to simplify the laser beam steering and focusing. The proposed system can be useful in many practical applications, such as providing ultra-high-speed and low-latency communications to users inside meeting rooms, offices, train stations, stadiums, airports and hospitals. Potential examples can include providing ultra-high-definition images of medical treatments in hospitals or of cloud robotics in smart manufacturing to a cloud for further processing.

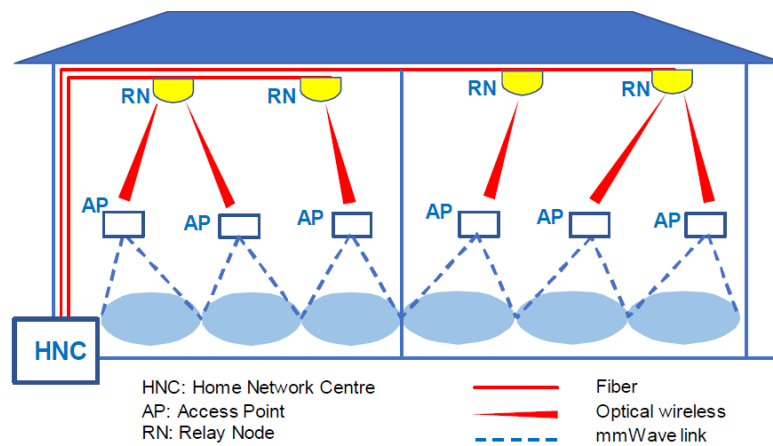


Fig. 42. Concept of the proposed hybrid system.

**Experimental demonstration**

The experimental setup for the transmission of a radio signal over a seamless fiber–OWC–mmWave system is presented in Fig. 43. First, a coherent two-tone optical signal with a frequency separation of 91.6 GHz is generated using a high-precision optical modulation technology. The two optical sidebands are separated, and one of them is modulated by orthogonal frequency-division multiplexing (OFDM) signals. The OFDM signals consisting of 512 subcarriers at 7.5 GHz are generated from an arbitrary waveform generator to modulate the optical signal using an optical in-phase/quadrature modulator. The

modulated optical signal is amplified and filtered to reduce the noise. The signal is thereafter re-combined with the unmodulated optical sideband using a 3-dB optical coupler. The combined optical signal is transmitted over a 20-km SMF to an optical receiver located at an RN. At the RN, the received optical signal is inputted to an optical collimator and an optical wireless signal is directly emitted into free space. After being transmitted over approximately 1 m in free space, the optical wireless signal is received using an objective lens at an AP. In this proof-of-concept experiment, we focused the optical wireless signal into an SMF. The focused signal is amplified, filtered, and inputted into a highspeed PD for being upconverted to an mmWave radio signal at 99.1 GHz. The signal is filtered and amplified before being transmitted into the air using a 23-dBi horn antenna. After being transmitted over approximately 1 m radio link in free space, the signal is received by another horn antenna located at the user end. The signal is amplified and down-converted to the microwave band using an electric mixer. Finally, the signal is sent to a real-time oscilloscope and is demodulated offline.

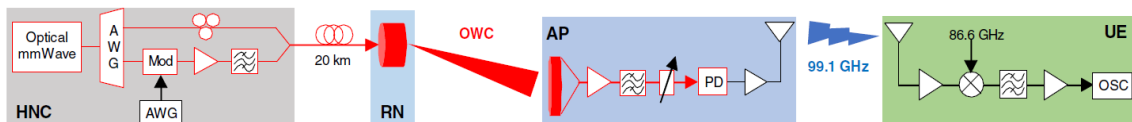


Fig. 43. Experimental setup for the proof-of-concept demonstration.

Figure 44 presents the performance of the signals after being transmitted over the system. Fig. 44 (a) shows the optical spectrum of the generated optical mmWave signal, consisting of the unmodulated and modulated sidebands with a frequency separation of 99.1 GHz. We evaluated the signal performance using the error vector magnitude (EVM) parameter. In the experiment, we generated OFDM signals having a bandwidth of 10 GHz and 8 GHz for 16-QAM and 32-QAM signals, respectively, and transmitted them over the system. The signals with a total capacity of 40 Gb/s were successfully transmitted over the systems. Satisfactory performance with EVM values meeting 7% forward error correction limits for all signals can be observed. Examples of constellations and spectral of the received signals at the user are shown in Fig. 44(c). Notably, the transmission distance of the OWC and mmWave links was limited to approximately 1 m in the experiment owing to the space limitations in the experiment room. The distances can be further extended to meet the requirement in practical systems. In addition, large-coupling-area PDs and PD arrays can be developed to simplify the coupling of optical wireless signals at the APs before converting them to mmWave access signals.

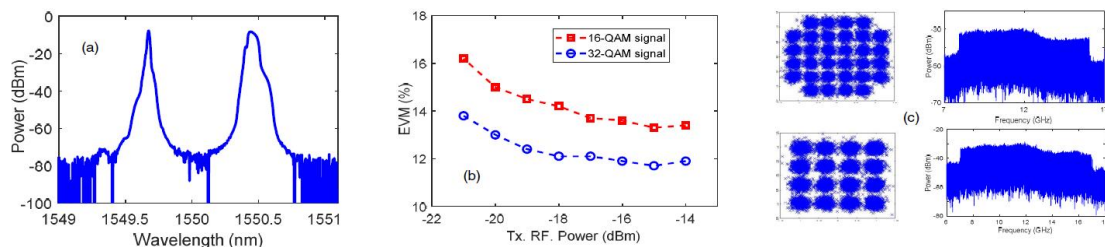


Fig. 44. (a) optical spectrum of the optical mmWave signal; (b) EVM performance; (c) constellations and spectral of the OFDM signals.

## F. Measurement Sensor

### System design and measurement method

Measurement and monitoring the quality of water, which is highly polluted in developing countries such as Indonesia and Vietnam, is an important issue for daily life and production. In these applications, a sensor is a fundamental and crucial component. Low-cost, low-energy consumption, accurate and multi-purpose sensors are highly demanded. Currently, there are three main sensing methods, including conductivity, absorptionmetric, and spectroscopy. However, there are several drawbacks with these methods, including regular cleaning and changing the probes, insufficient information to isolate and estimate the concentration of several types of particles or ions, and bulky and expensive. It is thus not easy for normal people, especially farmers in coastal saline lands, to own such a sensor for measuring the quality of air and water in their daily life and water quality in their production such as on coastal shrimp farms. In this project, we developed a non-invasive optical sensor using visible light spectrum. For our purposes, extracted features of absorption spectra were required. The measurement prototype had to be simple in design yet robust against measurement noises and artifacts. Furthermore, the system had to work in-situ, i.e. measurement on site, with minimum calibration requirement and human intervention. The design consisted of several blocks as shown in Fig. 45.

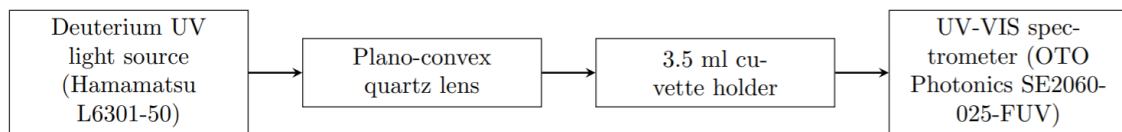


Fig. 45. Block diagram of the measurement system.

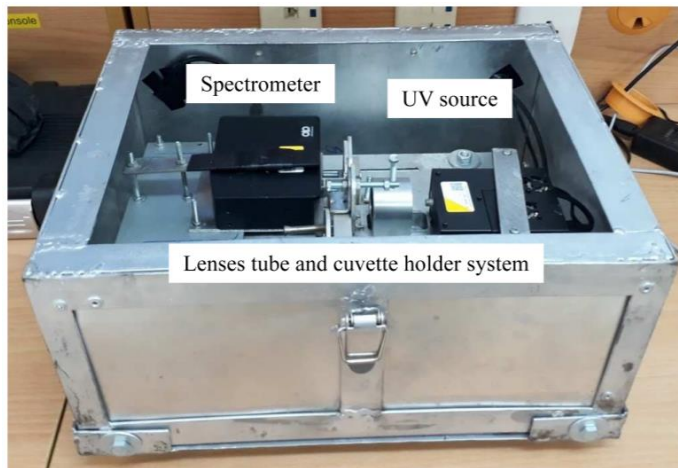


Fig. 46 . Prototype of the measurement system.

The first block was a commercial Deuterium UV light source from Hamamatsu (L6301-50). The radiated spectrum was non-uniform from 180 nm to 400 nm. The second block was a collimating lens to align the radiation beam through a cuvette holding slot. Since the half power beam width of the light source was  $15^\circ$ , the lens was a plano-convex lens with focal point  $f = 35.1$  mm and radius  $r = 25.4$  mm. For maximum throughput and minimum internal reflection error, the lens was a quartz lens with anti-reflection coating. The cuvette holding slot was designed to house standard 3.5 ml rectangular quartz cuvette with light path length

$l = 1$  cm. Finally, the third block was a commercial UV-VIS spectrometer from OTO Photonics (SE2060-025-FUV). The spectrometer could collect data from 180 nm to 850 nm with resolution around 0.4 nm. The spectrometer's detector was a Hamamatsu back-thinned charge coupled device (S10420-1106) with signal to noise ratio around 500. The whole system was arranged inside a closed metal box created by a computer numerical control (CNC) machine in the laboratory to prevent UV radiation leakage. The prototype of the developed system is shown in Fig. 46. Electronic circuits for driving and controlling the system were also realized and integrated into the system in the laboratory.

Throughout this work, we used normal letters, lowercase boldface letters, and uppercase boldface letters for scalars, vectors, and matrices, respectively. Measurement principles were based on Beer-Lambert's law. The received absorption intensity  $I$  of a solution can be expressed as:

$$I = I_0 10^{\sum_i -\epsilon_i c_i l}$$

where  $I_0$  is the incident light intensity (points),  $l$  is the light path length (cm),  $\epsilon_i$  (l/mol.cm) and  $c_i$  (mol/l) are the molar attenuation coefficient and concentration of the  $i$  components, respectively. In our system, we used a modified model to account for various sources of noise as follows:

$$I = k I_0 10^{\sum_i -\epsilon_i c_i l} + n.$$

The notation  $k$ , named systematic error, represented measurement errors that could not be reduced by averaging. Examples of these errors included, but were not limited to, non-uniform radiation intensity, different cuvettes, imperfection of cuvette surface, light beam displacement, and obliquity. The notation  $n$ , named random error, represented measurement errors that could be reduced by averaging. Examples of these errors included quantum noise and thermal noise.

The random error  $n$  was eliminated first by averaging. To ensure small statistical error, a large number of intensity values were collected at each wavelength in each measurement epoch before averaging. To mitigate the systematic error  $k$ , alternative measurement method was used. The measurement procedure was as follows:

- Add 3 ml of doubly distilled water to a quartz cuvette
- Measure absorption intensity for 2 minutes
- Calculate the average absorption intensity
- Withdraw all doubly distilled water from the quartz cuvette
- Add 3 ml of sample solution to the same quartz cuvette
- Measure absorption intensity for 2 minutes
- Calculate the average absorption intensity
- Divide the two sets of average intensity

By dividing the later to the former spectrum intensity,  $k$  could be reduced. Since the same doubly distilled water was used as reference, differences in absorbance feature between

bottled water samples could be distinguished.

### **Artificial intelligence approaches**

#### *For concentration estimation*

Estimation of concentration of sucrose was carried through two main steps: calibration and prediction. In the calibration step, absorption intensity from sample of known concentration was measured. The absorbance ratio could be rewritten in a matrix form as:

$$\mathbf{G}. \mathbf{A} = \mathbf{c}\mathbf{K} + \mathbf{E}$$

where  $\mathbf{A} \in \mathbf{R}^{m \times n}$  was the common logarithm of intensity ratio at  $n$  wavelengths from  $m$  samples;  $\mathbf{c} \in \mathbf{R}^{m \times 1}$  was the known concentration in  $m$  samples;  $\mathbf{k} \in \mathbf{R}^{1 \times n}$  was the ratio between absorbance of sucrose and doubly distilled water at  $n$  wavelengths; and  $\mathbf{E} \in \mathbf{R}^{m \times n}$  was the residual error. If there had been no error  $\mathbf{E}$ , the absorbance could have been found by solving for  $\mathbf{k}$ . Then, in the prediction step, an unknown concentration could be estimated by solving for  $\mathbf{c}$ . Traditionally, linear regression methods such as partial least square (PLS) are used.

However, in cases where the relation between received intensity and concentration is nonlinear, further error analysis should be used. In this work, three nonlinear methods using artificial intelligence were implemented to solve the above equation with error  $\mathbf{E}$ . The methods were artificial neural networks (ANN), principle component analysis with ANN (PCA-ANN), and genetic algorithm (GA). The key difference in these approaches was the assumption about residual error  $\mathbf{E}$ . With ANN, there was no assumption. With PCA-ANN,  $\mathbf{E}$  was assumed to be distributed in all dimensions. With GA,  $\mathbf{E}$  was assumed to be collinear in some dimensions.

#### *For sample classification*

For sample classification, we proposed the used of convolutional neural network (CNN). The unique characteristic of CNN is the convolution and pooling block, where each layer generates a successively high-level abstraction of a multi-dimensional input data. After the convolution and pooling block, the remained essential yet unique information is flattened to one dimension and processed with a fully connected neural network. CNN is commonly used for image and speech processing to capture the spatial and temporal dependencies of the data.

### **Experimental results for concentration estimation**

After applying our noise cancellation approach, extracted features of  $\text{NO}_2$  are shown in Fig. 47. In the figure, the absorbance feature followed of each concentration can be clearly distinguished. Consequentially, the concentration of  $\text{NO}_2$  can be estimated as shown in Fig. 48 using PLS.

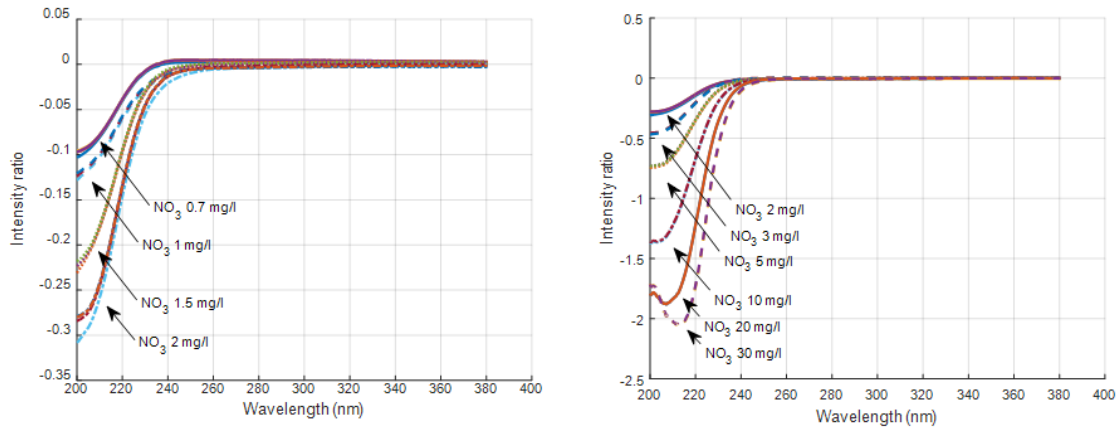


Fig. 47. Extracted features of NO<sub>2</sub> at different concentrations

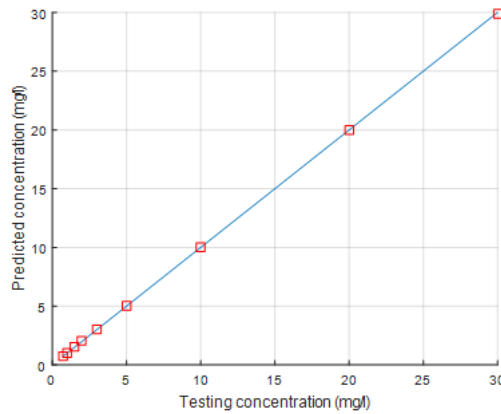


Fig. 48. Concentration estimation of NO<sub>2</sub>

In another case with sucrose, the extracted features were nearly the same. By applying artificial intelligence approaches, we were able to perform prediction with high accuracy. The extracted features and estimation results are shown in Fig. 49 and Fig. 50.

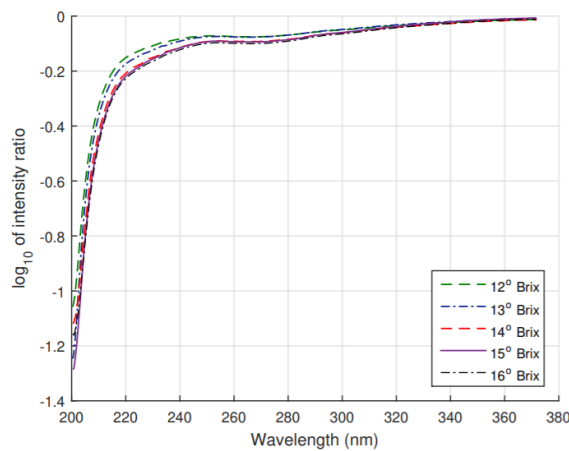


Fig. 49. Extracted features of sucrose at different concentrations

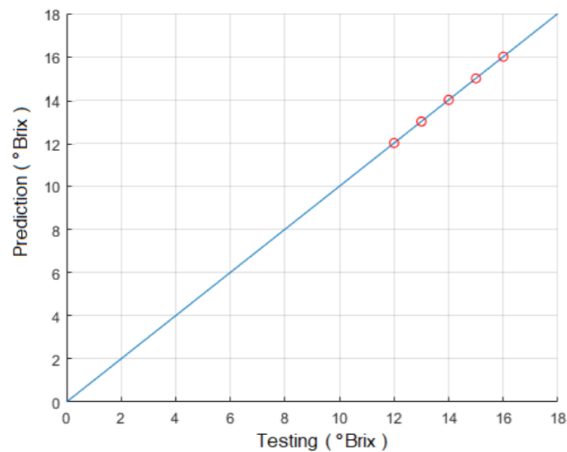


Fig. 50. Concentration estimation of sucrose

Experimental results clearly indicated that using the correct samples and wavelengths for calibration were of utmost importance. This might be the reason ANN cannot converge in some published articles. The assumption of the best method, i.e. GA, was that residuals were highly collinear in some particular dimensions. From experimental results, it indicated that the remained noise in the measurements was systematic errors. The error may be caused by impurity or other undiscovered sources in the prototype. Nevertheless, the approaches applied in this article provided extremely useful information for testing and improving spectroscopy sensing system such as our prototype.

**Experimental results for sample classification**

Bottled waters from five popular branches in Vietnam were used in the experiments. In order to avoid possible conflict of interests, the branches were anonymously labeled from A to E in this article. The bottles were randomly bought from several convenient stores around the university. Additionally, tap water was used as “counterfeit” bottled water. Since the bottled water and tap water samples were transparent to human’s eyes, it was impossible to identify the origin of the sample without prerequisite knowledge. Without our alternative measurement approach, the received intensities for each branch are shown in Fig. 51. The received intensities were nearly identical. With our noise cancellation approach, the extracted features of all branches are shown in Fig. 52. The absorbance features were highly collinear. If only the peak values had been used for analysis, the branches in each group could have been wrongly estimated as less concentration samples of each other. The output prediction using CNN are shown in Table VII. As shown in the table, prediction probabilities were higher than 0.99 in all cases. The results indicated that after the CNN had been trained to recognize a bottled water sample, it could accurately identify the origin of the testing sample. In other words, our proposed system could be used to quickly track an unknown bottled water product. Since each branch of bottled water had a different price, this capability would be extremely useful to double-check at the buyer side. When the bottle was filled with other source of water, the CNN could accurately identify the fraud. For example, when water sample from branch D was substituted by tap water in our experiments, the prediction probabilities could clearly show the change. Even if the features of D and tap water were highly collinear, probability that the sample was from branch D dropped to nearly 0%.

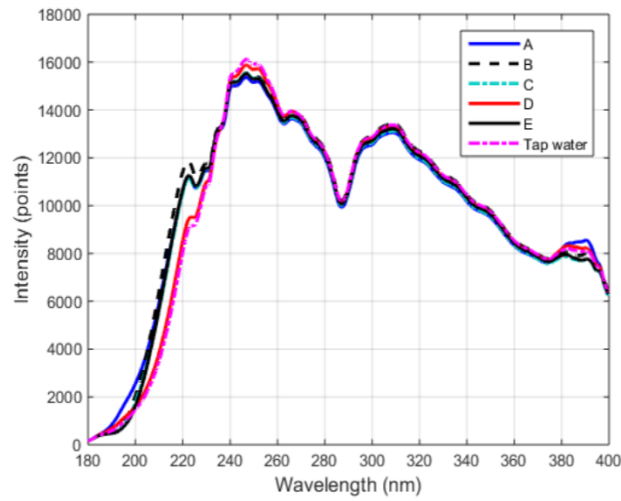


Fig. 51. Received intensity of bottled water samples.

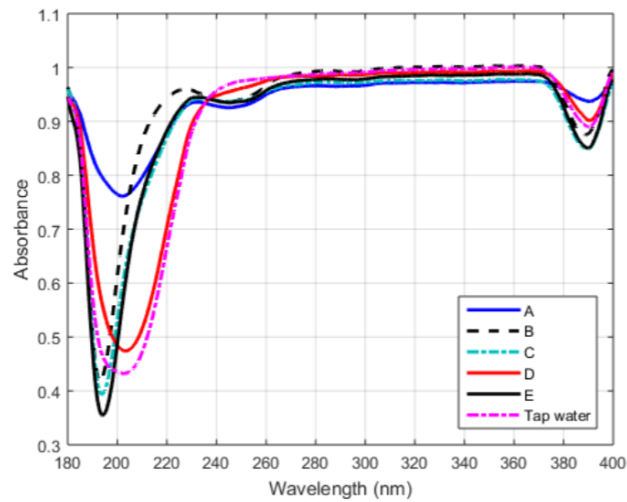


Fig. 52. Absorbance of bottled water samples.

Test sample	Output prediction probability					
	<i>A</i>	<i>B</i>	<i>C</i>	<i>D</i>	<i>E</i>	<i>Tap water</i>
<i>A</i>	0.998	0	0.002	0	0	0
<i>B</i>	0	0.998	0	0	0	0.002
<i>C</i>	0	0	0.998	0.002	0	0
<i>D</i>	0	0	0.003	0.996	0.001	0
<i>E</i>	0	0	0	0.001	0.999	0
<i>Tap water</i>	0	0.003	0	0	0	0.997

TABLE VII. PREDICTION RESULTS

## **(2) Leveraged Resources and Participants**

There are several reasons for the collaboration in this project, including:

- To share the knowledge and experience in this emerging and exciting field
- To share the facility and experiment conditions between the institutes
- To conduct proof-of-concept and field demonstrations for different use cases
- To promote the developed technologies to academia, industry, and practical applications in different countries.

The collaboration between the institutes helps enhancing the technical and social impacts of the project. The detail of each member 's contribution is described as follows,

- (i) National Institute of Information and Communication Technology: collaborates with other members to develop a mobile visible light communication system, a highly secured multiple-input multiple-output visible light communication system, and an ultra-high-speed indoor optical wireless system.
- (ii) Ho Chi Minh City University of Technology: developed organic-based visible light communications for internet of things application and the on-invasive optical sensor for water quality measurement. They hosted a project meeting in Ho Chi Minh city, and organized a workshop on related technologies of this project at an international conference.
- (iii) Indonesian Institute of Sciences: developed a low-speed visible light communication system for internet of things applications using low-cost devices and equipment. They also attended the IVO Forum 2019 and reported the project progress to the steering committee on behalf of the project.
- (iv) Posts and Telecommunications Institute of Technology: developed a secured quantum key distribution visible light communication system, and the networking aspect for visible light communication systems. They also hosted a project meeting in Hanoi and organized a lab tour in PTIT.
- (v) Chiang Mai University: developed the indoor localization system using visible light technology. They also hosted a workshop on visible light communications at an international conference in Chiang Mai city.
- (vi) Danang university of technology: developed digital signal processing for ultra-high-speed indoor communications and collaborated on the experiments. They also hosted a project meeting in Danang city and organized a Lab tour at the Danang university of technology.

In addition, all the members actively presented the project results to international conferences and/or published the results to international journals.

### **(3) Findings and Outcomes**

In this project, we have developed and achieved significant outcomes that can have high impact on the technology development and application in the fields of visible light and optical wireless communications. The significant findings and outcomes are summarized as follows,

- (i) The first end-to-end smartphone visible light communications: with the revolution of digital economy and social networks there has been a strong surge in demand for short range data communications and contactless payment (mobile Commerce) via Smartphone platforms due to their highly mobility and convenience. Existing wireless communications technology using radio frequency signals, such as Bluetooth, WiFi and near field communications has provided a ubiquitous communications environment for a wide range of mobile applications and digital services. Despite the benefits, radio frequency technology is, however, vulnerable to a myriad of threats and interference from other sources. This project developed the design and implementation of a complete screen to camera visible light communication system, where different personal devices were used for transmitting and receiving data (smartphones and tablets).
- (ii) Highest spectral efficiency organic LED based visible light communication system: by combining a newly developed pre-emphasis circuit and advanced modulation methods, we demonstrated a new organic LED based visible light communication system capable of achieving bandwidth efficiency of 286 bps/Hz, which was five times higher than state-of-the-art reports.
- (iii) The first cascaded optical wireless and millimetre-wave communication for ultra-high-speed and reliable indoor communication and a 40-Gb/s signal was successfully transmitted over a cascaded optical wireless and 100-GHz radio system. The system will be very useful for ultra-high-speed indoor communication in beyond 5G network with simple and easy alignment and tracking of user terminals.
- (iv) Ultra-high-speed indoor optical wireless communication of 100 Gb/s using wavelength-division multiplexing and Nyquist-subcarrier modulation for narrow laser beam system. The system can be further developed to achieve terabit per second class communication for future beyond 5G and 6G to facilitate the deployment of emerging broadband services, such as VR, haptic and holography.
- (v) In addition, the pioneering research efforts on networking and security aspects of visible light communications

### **(4) Broader Impact**

The developed technologies in this project can help to resolve emerging social problems, especially to ASEAN countries. The output social benefits of this project include:

- (i) Provide high-quality services and communications to both developed and developing countries: the developed systems can be applied to provide high-speed and real-time services for IoT applications and home networks. It would be very useful for applications in electromagnetic sensitive areas such as in aircraft cabins, hospitals and nuclear power plants. It also has a great potential to be applied in future communication networks such as 5G and beyond, and intelligent transportation and self-driving systems. The low complexity of our proposed solutions can help to save energy and cost and can be used in the areas where the electric power supply is limited.
- (ii) Solve emerging societal issues in ASEAN countries: for developing countries, such as Vietnam and Indonesia, water pollution is an important and urgent issue in developing countries. Our developed optical sensors can provide a cost-effective means for people, especially farmers in coastal saline lands, to monitor the quality of water for their daily life and production.

### **(5) Future Developments**

This project has been developing important technologies for future communications and applications, including for internet of things and future broadband mobile network. It is anticipated that visible light and infrared spectrum will play a vital role in future beyond 5G and 6G network to compliment the traditional radio-based communications. In this project, we have developed both low cost visible light communications for mobile applications, such as contactless payment, and for internet of things, and localizations. The organic LED based visible light communications are very promising owing to its low cost, high energy efficiency. We also developed ultra-high-speed indoor optical wireless communication with an achieved data rate of 100 Gb/s. In the field of access networks, 5G is being studied and tested worldwide, however, it can only meet the requirements for the next 10 years. Mobile traffic keeps growing and the overall mobile data traffic can reach 5 zettabytes per month by 2030. The need for more bits, more spectrum, and higher network densification to support unprecedented demands for new services, such as haptic communication, high-fidelity virtual and augmented realities, virtual meeting rooms, networked games, and smart healthcare, require the wireless network to provide at least Terabits/second aggregated bit rate in small regions. To cope with the unprecedented data growth and other quality requirements in the next decades, necessary steps are highly needed to boost the research effort. Compared to the current networks, including those of 5G network, a paradigm shift in the design and operation of radio access and transport networks must be considered. Exploring ultra-dense small cells using radio signals in very high frequency regions ranging from the conventional microwave to sub-terahertz and lightwave bands, can be the key technologies. Thus, our developed technologies in this project can be further extended to reach data rate necessary for future applications. After the project is completed, we will continue our research collaborations to develop new systems and demonstrations with higher data

rate and provide a better coverage. We will present the research outcomes to international conferences, publish at international journals, and especially, consider contributing to international standardizations.

### **iii) Social Contribution**

In this project, we actively promoted the research results to academia, including presenting the results to international conferences, and publishing the results to international journals. We also organized many project meetings and hosted many workshops and special sessions at the international conferences to spread out the research outcomes international community. The publications related to this project are listed as follows,

#### **Journal papers**

[J1]. O. I. Younus, H. L. Minh, P. T. Dat, N. Yamamoto, A. T. Pham, and Z. Ghassemlooy, "Dynamic Physical-Layer Secured Link in a Mobile MIMO VLC System," IEEE Photonics Journal, April 2020, Accepted.

[J2]. Ngoc T. Dang and Vuong V. Mai, "A PHY/MAC Cross-Layer Analysis for IEEE 802.15.7 Uplink Visible Local Area Network" IEEE Photonics Journal, vol. 11, no. 3, p. 7903517, 2019.

#### **International Conferences**

[C1]. Pham Tien Dat, Nguyen Tan Hung, Mitsuji Matsumoto et al., Hybrid FSO/mmwave system for high-speed and reliable mobile fronthaul, Proc. 45th European Conference on Optical Communication" (ECOC 2019), Dublin, Ireland, September 2019.

[C2]. Pham Tien Dat, Atsushi Kanno, Keizo Inagaki, Toshimasa Umezawa, Naokatsu Yamamoto, and Tetsuya Kawanishi, Hybrid Optical Wireless-mmWave: Ultra-High-Speed Indoor Communications for Beyond 5G, IEEE INFOCOM 2019-IEEE Conference on Computer Communications Workshops (INFOCOM WKSHPs), Paris, France, April 2019.

[C3]. Nghi Vinh Khanh, Pham Quang Thai, Vu Dinh Thanh, "Comparison of modulation methods for visible light communication system using organic LED", ICSPCS 2019, Australia, 2019.

[C4]. Pham Quang Thai, Pham Tien Dat, "Brix percentage estimation using artificial intelligence approaches", In the Proc of the 4th International Conference on Photonics Solutions (ICPS2019), Chiangmai, Thailand, Nov. 2019.

[C5]. Ngoc T. Dang, Minh B. Vu, Thu A. Pham, Hien T. T. Pham, and Vuong V. Mai, "Quantum Key Distribution Solution over Visible Light Communication Networks" In the Proc of the 4th International Conference on Photonics Solutions (ICPS2019), Chiangmai, Thailand, Nov. 2019, pp. 113310A.1-113310A-9.

[C6]. Rattakorn, P., Mankong, U., Potha, S., "Three-dimensional VLC indoor positioning system using smart device camera receiver with image processing technique," in Proceedings of SPIE - The International Society for Optical Engineering, Volume 11331, 2020.

[C7]. Pham Quang Thai, Pham Tien Dat, "Counterfeit bottled water detection using

absorption spectroscopy and convolutional neural networks”, MORSE, Indonesia, 2019.

[C8]. Hubert Dzieciol, Hoa Le Minh, Zabih Ghassemlooy, Pham Tien Dat, Son The Tran, “Comparative Study of Image Processing Performance of Camera-Based Visible Light Communication Using Android Acceleration Frameworks,” 2018 11th International Symposium on Communication Systems, Networks and Digital Signal Processing, CNSDSP 2018.

[C9]. Pham Quang Thai, Francois Rottenberg, Pham Tien Dat, Shimamoto Shigeru, Increase Data Rate of OLED VLC System Using Pre-Emphasis Circuit and FBMC Modulation, OSA Imaging and Applied Optics Congress, Orlando, FL - United States, 2018.

[C10]. Pham Quang Thai, Filter Bank Multi-carrier and Non Orthogonal Multiple Access in MIMO OLED VLC System, Progress in Electromagnetics Research Symposium (PIERS), Toyama - Japan, 2018.

[C11]. Mitsuji Matsumoto, Trend of high-speed optical wireless system, In the Proc of the PIERS2018, Special session on “Optical Wireless Technologies for Mobile Communications and Internet of Things”, Toyama, Japan, Aug. 2018 (Invited).

[C12]. Yusuf Nur Wijayanto, Pham T. Dat et al., Short Range Visible Light Communication for Data Transfer Using Simple Optoelectronic Circuits, PIERS2018, Toyama, Japan, Aug. 2018.

[C13]. Nguyen T. Hung, Pham T. Dat et al., Chaos-secured Software-defined Visible Light Communications, PIERS2018, Toyama, Japan, Aug. 2018.

[C14]. Nguyen T. Hung, Pham Q. Thai, P. T. Dat, Smart lighting for internet of things and smart homes, ICCE 2018, Hue, Vietnam, July 2018 (Invited).

[C15]. Ngoc T. Dang, “Relay-assisted VLC Networks Using Code Division Multiple Access and Analog Network Coding” In the Proc of the PIERS2018, Special session on “Optical Wireless Technologies for Mobile Communications and Internet of Things”, Toyama, Japan, Aug. 2018.

[C16]. Mankong, U., Potha, S., Srisang, P., “Comparison of Indoor Positioning System Techniques Using Visible Light Communication,” Progress in Electromagnetics Research Symposium, PIERS2018, Toyama, Japan (Abstract only).

[C17]. Mitsuji Matsumoto, Overview of Optical Wireless Communications, The 2017 International Symposium on Electrical and Electronics Engineering, Ho Chi Minh City, Vietnam, November 2017 (Invited).

[C18]. Yusuf Nur Wijayanto, Short-Range Visible Light Communication with Low-Cost Devices for Smart Homes, The 2017 International Symposium on Electrical and Electronics Engineering, Ho Chi Minh City, Vietnam, November 2017.

[C19]. Pham Quang Thai, Pre-Emphasis Circuit for OLED VLC Systems, The 2017 International Symposium on Electrical and Electronics Engineering, Ho Chi Minh City, Vietnam, November 2017.

[C20]. Vuong V. Mai, Ngoc T. Dang, Truong C. Thang, and Anh T. Pham, Hybrid VLC/WIFI Networks: CSMA/CA-based MAC Protocol Design and Performance Analysis, The 2017 International Symposium on Electrical and Electronics Engineering, Ho Chi Minh City, Vietnam, November 2017.